Extreme longevity of highly fecund termite queens achieved by mitochondrial and insulin upregulation without harmful lipid signatures or accumulation

Sarah Séité[1, 2#], Mark C. Harrison[3#], David Sillam-Dussès[4], Roland Lupoli[1, 2], Tom J. M. Van Dooren[5, 6], Alain Robert[4], Laure-Anne Poissonnier[7], Arnaud Lemainque[8], David Renault[9, 10], Sébastien Acket[11], Muriel Andrieu[12], José Viscarra[13], Hei Sook Sul[13], Z. Wilhelm de Beer[7], Erich Bornberg-Bauer[3] and Mireille Vasseur-Cognet[1, 2, 14*]

1- UMR IRD 242, UPEC, CNRS 7618, UPMC 113, INRAe 1392, Paris 7 113, Institute of Ecology and Environmental Sciences of Paris, Bondy, France.

2- University of Paris-Est, Créteil, France.

3- Institute for Evolution and Biodiversity, University of Münster, Münster, Germany.

4- Sorbonne University Paris Nord, Laboratory of Experimental and Comparative Ethology UR4443, Villetaneuse, France.

5- UMR UPMC 113, IRD 242, UPEC, CNRS 7618, INRA 1392, PARIS 7 113, Institute of Ecology and Environmental Sciences of Paris, Paris, France.

6- Naturalis Biodiversity Center, Leiden The Netherlands.

7- Department of Biochemistry, Genetics and Microbiology, Forestry and Agriculture Biotechnology Institute, University of Pretoria, Pretoria, South Africa.

8- Genoscope, François-Jacob institute of biology, Atomic energies Agency, University of Paris-Saclay, Evry, France.

9- University of Rennes, CNRS, ECOBIO (Ecosystems, biodiversity, evolution) - UMR 6553, Rennes, France.

10- University Institute of France, Paris, France

11- University of Technology of Compiègne, UPJV, UMR CNRS 7025, Enzyme and Cell Engineering, Royallieu research Center, Compiègne, France.

12- Cochin Institute, UMR INSERM U1016, CNRS 8104, University of Paris Descartes, CYBIO Platform, Paris, France.

13- Department of Nutritional Sciences and Toxicology, University of California, Berkeley, USA

14- INSERM, Paris, France

* Correspondence and requests for materials should be addressed to MVC

email: mireille.vasseur@inserm.fr

https://orcid.org/0000-0001-6963-4114

#These authors contributed equally

ABSTRACT

Eusocial termite queens achieve nearly maximal fertility throughout their extremely long life without apparent signs of aging. Termites represent, therefore, an ideal model for aging research. To investigate the molecular mechanisms underlying their long reproductive life, we carried out transcriptomic, lipidomic and metabolomic analyses on fat bodies of sterile short-lived workers, long-lived kings and five stages spanning twenty years of adult queen maturation. In mature reproductives, genes supporting a robust mitochondrial functioning or associated with genome stability were upregulated. In most organisms, insulin signaling increases fertility but decreases lifespan, often accompanied by harmful lipid signatures. Our findings suggest that an upregulation of insulin-like peptide (Ilp9) in the fat body of termite queens is accompanied by a specific lipid metabolism, limiting fat storage, thus sustaining both high fertility and maintaining extreme lifespan. Our results highlight potential molecular targets for research into aging-related metabolic diseases linked to the accumulation of excess fat.

INTRODUCTION

Aging affects almost all living organisms. It is characterized by the failure of several cellular and physiological functions. This often leads to a deleterious accumulation of lipids[1], while a reduction in mitochondrial functioning exacerbates oxidative stress[2]. In most multicellular organisms, surgical or genetic interventions which reduce fecundity can increase lifespan[3], suggesting that fecundity and longevity are negatively correlated[4,5]. This pattern is usually explained by a trade-off, where resources allocated to fecundity are no longer available for somatic maintenance and thus survival[4,6,7]. However, the regulatory mechanisms and signaling pathways controlling the allocation of resources in this trade-off remain insufficiently understood[8].

Our understanding of the causes of aging stems to a large extent from studies on short-lived model organisms[9,10]. Eusocial insects such as the fungus-growing termite *Macrotermes natalensis* (Termitidae, Blattodea) have reproductive castes which outlive their sterile siblings by orders of magnitude despite having the same genome[11–13]. Queens lay thousands of fertile eggs per day[14], and both queens and kings can live for several decades, while workers live for only a few weeks. Long-lived termite queens seem close to their maximum possible fertility for a prolonged time without apparent signs of aging and thus with a negligible cost of reproduction[15]. Among social insects, termites are an excellent new natural model system for aging research. Several molecular mechanisms involved in bypassing the fecundity/longevity trade-off have been identified in social insects, but their integrated physiological effects remain poorly understood[15–19].

Recently, transcriptomic studies in different taxa of social insects have pointed out the importance of downstream components of the Insulin/insulin-like growth factor (IGF-1) signaling (IIS) and target of rapamycin (TOR) network for aging [20–22]. IIS and TOR signaling have been broadly identified as key actors in the allocation of resources and aging of

77 organisms[23]. IIS is an evolutionarily conserved pathway which controls food intake, energy
78 stores, energy expenditure, growth and fecundity via the IRS–PI3K–AKT signaling cascade
79 which targets, in particular, TOR complex 1 (TORC1), inducing protein translation and *de novo*
80 lipogenesis[24]. In *Drosophila*, a reduction of the activity of IIS or TOR pathways can extend
81 lifespan substantially while reducing female fecundity[25–27]. Beyond the influence of these two
82 signaling pathways on fecundity in *Drosophila*, dysregulation of the IIS or TOR pathways, for
83 instance by the impairment of lipid metabolism, leads to the development of metabolic, age-
84 related pathologies from *Drosophila* to humans, such as type 2 diabetes and insulin
85 resistance[28,29].

86 Physiological consequences of differences between social insect castes in IIS and TOR
87 pathways and targets have thus far not been assessed using metabolomics or lipidomics. The
88 fat body, which acts like the mammalian liver and white adipose tissue, is central for
89 intermediary metabolism and energy balance in insects[30,31]. In *Macrotermes* termites, two
90 castes with different reproductive roles (queens and kings) live up to high age and can be
91 compared with short-lived castes. This permits a separation of shared lifespan prolonging
92 mechanisms from those that differ between the sexes. Some differences can be attributed to
93 sex-specific reproductive roles and could help to understand the absence of a cost of
94 reproduction in females or in both sexes. Whereas a gene expression module has been proposed
95 to characterize "queen-ness" (QCM) in termites, the analysis did not account for properties
96 shared with kings[21]. Neither have the fat bodies of kings and queens of highly eusocial termites
97 been investigated.

98 We studied *M. natalensis* abdominal fat bodies of five queen reproductive stages (adult
99 virgin to twenty-year-old queen), long-lived reproductive kings and short-lived,
100 nonreproductive female workers. We identified multiple biological pathways affecting aging
101 through OMICS analyses. In queens and kings, an anticipated downregulation of the TORC1

signaling occurs but also an unexpected 800-fold upregulation of an insulin-like peptide gene which we called *Ilp9*. The upregulation of the *Ilp9* gene coincides with high glucose levels in the hemolymph of mature queens. This apparent insulin increase is associated with an upregulation of gene programs involved in the synthesis of proteins and specific lipids with low oxidation potential, destined for oogenesis rather than fat storage. We were able to link this phenomenon to a non-canonical downregulation of a gene coding a diacylglycerol acyltransferase (*midway*; *mdy*) in mature reproductives. Consistent with transcriptomic data, lipidomic analyses in the fat body of queens demonstrated a decrease in the concentration of preferentially stored lipids (triglycerides) and an increase in the concentration of lipids destined for oogenesis (diglycerides). Furthermore, we observed an upregulation of genes supporting a robust mitochondrial functioning and of aging-related genes associated with genome stability which may drive their long-lifespan.

RESULTS

Analysis of gene expression patterns in fat bodies

Macrotermes natalensis queens (QT4) and kings (KT4), which were over 20 years old, and short-lived female (minor) workers (FW) were sampled in field colonies in 2016 and in 2018. Incipient colonies were each founded from one male and one female imago (T0) collected in the field and raised for 31 months following a protocol based on the natural life history of *Macrotermes* species[32,33] (Fig 1a and Methods). Queens of these laboratory colonies were sampled at 3 months of age (QT1), 9 months (QT2) and 31 months (QT3). To investigate how caste and sexual maturity affect gene expression, we analysed a total of 25 transcriptomes of abdominal fat bodies. Sterile female workers FW, queens QT0-QT4 and mature kings KT4 were each sampled from at least 3 independent colonies (Fig. 1a). RNA-sequencing data showed that variation in expression between castes was greater than between replicates

(Principal Component Analysis, PCA of top 500 genes in terms of variance, Fig. 1b). This PCA showed that FW expression was very distinct from that of KT4 and all queen stages, with a strong separation along the first axis (52% variance explained). Removing FW expression from the PCA allowed a clearer separation of the reproductive individuals within the first two axes (58% variance explained). Four distinct groups were found: young queens (QT0 and QT1), QT2, KT4 and mature queens (QT3 and QT4) (Fig. 1b). We then carried out a signed, weighted gene co-expression network analysis[34]. The resulting gene co-expression network (GCN) allowed us to identify nine modules of particularly strongly co-expressed genes (Fig. 1c). We identified regions of the GCN that were up- or downregulated between castes or with queen age. In accordance with the PCA (Fig. 1b), we found modules strongly and uniquely correlated with FW (blue module, 1103 genes) and KT4 (plum1 module, 116 genes). One yellow module was upregulated in mature queens, QT3 and QT4 (yellow module, 537 genes). Finally, the light-cyan module (3455 genes) may be related to long-lived reproductives QT4 and KT4, though the latter only as a trend (KT4 0.39 $p = 0.05$). This largest of the modules was enriched for functions related to transcription and general protein synthesis. We subsequently tested for expression differences between specific pairs of castes or ages in all or a subset of individual genes.

Long-lived reproductives share expression patterns underlying remarkable lifespan

Despite their pronounced sexual dimorphism, the king and the queen in *M. natalensis* have similar longevity. A comparison of transcriptomic profiles in fat bodies of KT4 and QT4 with FW allows us to look at genes potentially underlying lifespan (Supplementary Fig.1), irrespective of reproductive efforts distinguishing kings from queens. A total of 1454 genes were upregulated in fat bodies of KT4 and QT4 including 350 genes that differed between KT4 and QT4. In addition, 2208 genes were downregulated in KT4 and QT4, 468 of which were

significantly different between KT4 and QT4. We observed significantly upregulated expression of components of IIS signaling in the fat bodies of KT4 and QT4 with *Ilp9* (800-fold increase), *pi3k59f* and two insulin targets *eIF6* and *crc*[35] (Fig. 2 and Supplementary Tables 1 & 2). These results were accompanied by the upregulation of gene expression involved in several processes related to protein and macromolecule synthesis (Supplementary Fig. 1). In contrast, the expression of *InR2* and several actors involved in the TORC1 signaling pathway (*tor*, *raptor* and its *S6K* substrate) were downregulated in QT4 and KT4, as well as the *mdy* lipid metabolism gene (Fig. 2 and Supplementary Tables 1 & 2). *Mdy* is a diacylglycerol acyltransferase gene coding an enzyme catalysing the final step of triglyceride (TG) synthesis from diglycerides (DG)[36]. This downregulation of the *mdy* gene suggests a decrease of fat storage in reproductives. Moreover, the expression of many genes important for genome stability, including genes involved in DNA damage response and telomere maintenance, was upregulated in KT4 and QT4 (Fig. 2 and Supplementary Tables 1 & 2). In addition, several genes coding for the OXPHOS systems and the mitochondrial ribosomal proteins, mitochondrial transport and mitochondrial fission were upregulated in QT4 and KT4 (Fig. 2 and Supplementary Tables 1 & 2). These results suggest that mitochondrial function was maintained in the fat body of long-lived reproductives with likely beneficial effects on cell integrity and oxidative status. Accordingly, we observed a downregulation of the expression of antioxidant genes in QT4 and KT4 compared to FW (Fig. 2 and Supplementary Table 1 & 2).

Together, these results suggest that long-lived reproductives share several expression differences from workers in agreement with a reduction or absence of aging, but also an unexpected upregulated expression of several components of the IIS pathway and a downregulated expression of *mdy* and antioxidant genes.

The fat body of highly fecund and long-lived queens indicates a specific energetic gene program

To better understand differences in metabolic gene programs which might be explained by mature queen reproduction and relate to the absence of costs of reproduction, we mapped the differentially expressed genes (DEGs) in the fat bodies of FW and QT4 to the GCN and focused on patterns where QT4 differ from FW and KT4, which oogenesis might explain. These DEGs occupied very distinct regions of the network, with genes upregulated in FW mainly contained within the blue, light-yellow and light-green modules and DEGs in reproductives mainly contained within light-cyan (Fig. 1c). Although reproductives have several DEGs in common, differences between KT4 and QT4 occur: genes contained in the plum module were specifically up-regulated in KT4 while genes in the yellow module were specifically up-regulated in QT4 (Fig. 1c). Upregulated gene expression in FW was centered around cell signaling and responses to stimuli, whereas gene expression in QT4 and KT4 was mainly related to macromolecule synthesis with higher protein production in the KT4 fat body (Fig. 1c and Supplementary Fig. 2). Several genes involved in IIS pathway were differentially regulated in QT4 relative to FW and KT4. *InR3 and pdk1* expression were upregulated in QT4 compared to FW, and downregulated in KT4 (Supplementary Table 3). *pi3k59f* and *crc* were more strongly upregulated in QT4 than in KT4 (Supplementary Table 2). In QT4, we also observed an upregulation relative to FW of *pi3k21b* genes encoding the kinases involved in the IIS pathway (Supplementary Table 2). In contrast, *pi3k92e* gene expression was downregulated in the fat body of QT4 relative to FW (Supplementary Table 2). In response to carbohydrates, insulin concentration increases and activates, via the IIS pathway, glycolysis and *de novo* lipogenesis and increase mRNA translation[35,37]. We found major differences in gene expression within carbohydrate and lipid metabolism pathways between QT4 and both FW and KT4. Several genes, located in the blue and light-green GCN modules and involved in the glycogenesis and

trehalose energetic storage pathways, were upregulated in FW (Supplementary Tables 1-3). Trehalose-6-phosphate synthase was upregulated relative to QT4, but not to KT4 (Supplementary Table 3). In QT4, on the other hand, several genes of the yellow and light-cyan GCN modules which are key players in carbohydrate catabolism were upregulated relative to KT4 and FW, particularly genes encoding enzymes involved in glycolysis (e.g. *cg6650* also known as *adpgk*, *pfk* and *pkm;* Supplementary Table 3), as well as hexosamine biosynthetic pathway (HBP) and pentose phosphate pathway (PPP) (Supplementary Tables 2 & 3). These were found next to those promoting fatty acid (FA) synthesis from carbohydrates (*acc* and *fasn1*; Supplementary Table 3). Interestingly, the expression of genes promoting FA activation, esterification and elongation was also upregulated in QT4 relative to KT4 and FW (Supplementary Table 3). Heightened DG transport in QT4 is suggested by an upregulation relative to FW and KT4 of expression of lipoprotein genes essential for oogenesis, such as the female-specific vitellogenin (*vg*) and the diacylglycerol-carrying lipoprotein (*hdlbp*) (Supplementary Tables 2 & 3).

Overall, the results of this comparison suggest that the metabolism of FW tends to facilitate energetic storage while the QT4 metabolism seems to be oriented towards the utilization of energy resources for reproduction (oogenesis), more strongly so than KT4.

Transcriptomic analysis of queens at different stages highlights adult developmental remodeling and expression changes within the highly fecund mature stage.

Concomitantly with the development of colonies, the imaginal fat body of virgin females (QT0) with fat storage tissue becomes replaced by a royal fat body (QT4) which is highly oriented towards specific protein synthesis and secretion[38]. Since endoreduplication (the replication of DNA during the S-phase of the cell cycle without subsequent cell division) was specifically

225 reported for the fat body of queen termites[39], we recorded polyploidization in the fat body
226 during queen maturation using flow cytometry. Moreover, to investigate the molecular
227 mechanisms involved in the establishment of the dedicated energetic metabolism in mature
228 QT4 and in the change of fat body identity with maturation, we compared gene expression
229 between adult females in five life stages (Fig. 1a). Different regions of the gene co-expression
230 network were upregulated in each stage (Fig. 3), and we focus on comparing expression
231 differences between adjacent stages.

232 First of all, the level of expression of *Ilp9*, *InR3* and *vg* genes was not different between
233 QT3 and QT4 (Supplementary Table 4 and Fig. 4). However, *crc* gene expression
234 (Supplementary Table 4) and genes involved in glycolysis and OXPHOS, mitochondrial
235 membrane transport proteins and mitochondrial ribosomes, were all strongly upregulated in
236 QT4 compared to QT3 (Supplementary Table 4). Accordingly, GO terms suggest an increase
237 of several processes linked to protein synthesis and secretion (Fig. 3). We can conclude from
238 this that among mature queen stages, substantial further upregulation of important processes
239 can occur with reproductive age and that these reinforce the energy metabolism discussed
240 above. In particular, mitochondrial functions seem to be upregulated substantially with age.
241 Other main aspects of mature queen metabolism might be present already in young queens,
242 before massive reproduction occurs.

243 Queens live several weeks without food after mating, due to a lack of workers which
244 feed all colony members[38]. The imaginal fat body of virgin females (QT0) at the start of this
245 starvation period displayed high expression of genes associated with intracellular signal
246 transduction, such as the superfamily Ras which notably controls cell growth. We observed that
247 *Egfr* gene expression and downstream signaling cascades, such as *Ras/Mapk* signaling were
248 upregulated in comparison to QT1 (Supplementary Table. 4). GO analysis revealed that several
249 signaling pathways involved in development and apoptosis were upregulated as well (Fig. 3).

Furthermore, within the IIS pathway, expression of *InR2*, *InR3*, *pi3k21b*, and *Akt1* were upregulated (Supplementary Table 4).

At the end of the starvation period (stage QT1), we observed an enrichment of GO terms related to an increase of catabolic processes (Fig. 3), an upregulation of genes involved in pathways linked to an increased use of reserves. More specifically we observed an upregulation of *Ampkα* gene expression (AMP-activated Protein Kinase α; Supplementary Table 4) known to be activated under conditions of low energy to redirect the metabolism and restore energy balance by inhibiting anabolic processes and promoting catabolic processes and mitochondrial functioning[40]. Consistent with the increase of *Ampkα* gene expression, we observed increased expression of genes involved in several catabolic processes such as β-oxidation and proteolysis (Fig. 3 & 4), as evidenced by the upregulation of several genes coding for subunits of the proteasome and autophagy and a decrease of anabolic processes such as lipogenesis (Supplementary Table 4 and Fig. 4). We observed further responses which can be explained as stress responses to starvation. AMPK is known to influence mitochondrial homeostasis by initiating both the degradation of damaged mitochondria and mitochondrial biogenesis[40]. We observed an upregulation of two genes involved in mitochondrial fission (*drp1* and *fis1*) known to facilitate mitochondrial degradation by autophagy and two genes involved in a specific degradation of mitochondria via autophagy called mitophagy, *cg5059* also known as *BCL2 interacting protein 3* and *pink1* (Supplementary Table 4). Moreover, we observed an upregulation of the expression of genes involved in the OXPHOS system, mitochondrial ribosome subunits and mitochondrial transport proteins, suggesting an increase in mitochondria biogenesis (Supplementary Table 4). Finally, we observed an increased expression of antioxidant genes (Supplementary Table 4) which are known to be upregulated by AMPK in situations of oxidative stress[41].

At QT2, antioxidant defense processes, as well as *Ampkα* gene expression, were downregulated again (Supplementary Table 4). At this stage, GO terms showed that several processes were linked to protein metabolism (Fig. 3). We believe that QT2 are fed by workers. This is consistent with the increase in the number of workers per colony (Supplementary Fig. 3b) and of fungus development (Supplementary Fig. 3c). *Ilp9*, *pi3k21b* gene expression, and *de novo* lipogenic genes were upregulated in QT2 compared to QT1, suggesting a first activation of IIS pathway components in the fat body of QT2 (Supplementary Table 4 and Fig. 4). At the same time, we observed a downregulation of *mdy* gene expression, even relative to the mature queen stages (Fig. 4). In addition, several genes involved in the cell cycle, including *mcm2, 5, 6, 7 and 10*, several cyclins and cyclin-dependent kinases, such as *cycE*/*cdk2* and *orc1*, and the proto-oncogene *myc* were up-regulated (Supplementary Table 4). Associated to these genes, we observed an increase in QT2 fat body endoreduplication levels, with the proportion of 4C nuclei now exceeding 70 % (Fig. 5) in comparison to 35% in QT0 and QT1. Taken together, these data suggest that QT2 is a transitory stage where maturation is prepared or initiated in many processes.

In QT3, the abdomen has become enlarged. During this period, expression of *Ilp9* and *InR3* genes was upregulated in comparison to QT2 whereas *InR2* gene expression decreased (Supplementary Table 4). We also observed an upregulation of genes involved in glycolysis, HBP and PPP (Supplementary Table 4). Similarly, the expression of genes involved in *de novo* lipogenesis, as well as FA activation, elongation, esterification and transport were upregulated (Fig. 4). This is in accordance with increased fertility and associated genes, such as *vg* (Fig. 4) and these expression patterns do not change further in QT4. We found that over 90% of all cells in the fat bodies of QT3 and QT4 have 4C nuclei (Fig. 5).

Overall, these data suggest that the energy metabolism of young queens shows many characteristics in accordance with their starvation period. With social nutrition (increase in the

number of workers and food availability), colony sizes increase. The QT2 stage acts as a transitional period where the energy metabolism of mature queens becomes established. This is associated with an upregulation of several specific insulin-signaling genes and a downregulation of genes involved in lipid storage (*mdy*). Other lifespan affecting processes seem to be initiated in QT2 (e.g., upregulation of IIS pathway components), or in QT4, long after maturation (e.g. upregulation of mitochondrial functions).

Major changes in metabolites and lipid composition in mature queens reflect their transcriptomes

We investigated hemolymph metabolomes in FW and queen maturation stages (QT0-QT4). Metabolomes differed between FW and QT4, and between each pair of successive queen maturation stages (pairwise perMANOVA each $p < 0.05$, Fig. 6). FW and QT0 seemed little different overall, while starved QT1 were well separated from the QT2 individuals in transition towards massive reproduction (Fig. 6). Physogastric QT3 were globally intermediate between QT0, QT2 and QT4 (Fig. 6). We compared individual metabolite concentrations between FW and QT4 and between successive queen maturation stages (Supplementary Figure 4 and Table 5). Glucose and galactose are the metabolites present in the largest concentrations in QT4. This high concentration of glucose[42] occurred similarly in FW but not in any of the younger queen stages. Surprisingly, the concentration of trehalose was lower in QT4 than in FW or in any other queen stage. Alanine, glycerol, aspartic acid, phenylalanine and glutamic acid occur in larger concentrations in QT4 than FW, corresponding with ongoing increased protein and lipid synthesis. Relative to QT0, starved queens QT1 have increased levels of leucine, threonine, isoleucine and citric acid, which decrease again in QT2 and are indicative of proteolysis during starvation.

323 The lipidomic analysis in hemolymph revealed eighty-one esterified lipid species of
324 which 34 differed in quantity and composition between FW and QT4 (Fig. 7 and Supplementary
325 Table 6). Strikingly, DG were significantly elevated in QT4 relative to FW while TG were
326 significantly diminished (Fig. 7 and Supplementary Table 6). Furthermore, we compared lipid
327 compositions between the fat bodies of young QT0, the transitional stage QT2 and QT4 mature
328 queens (Fig. 8a and Supplementary Table. 7). Thirteen TG concentrations were significantly
329 lower in QT4 relative to QT0 while other changes were often in the same direction as in
330 hemolymph. We investigated changes in PUFA/MUFA/SFA proportions in hemolymph of FW
331 and QT4 and in fat bodies of QT0, QT2 and QT4. In hemolymph, PUFA/MUFA/SFA
332 proportions were not significantly different between FW and QT4 (Fig. 7b). In contrast,
333 PUFA/MUFA/SFA proportions in fat bodies of QT2 and QT4 were significantly different from
334 QT0 (PERMANOVA, p-value < 0.05) (Fig. 8b). This difference seemed to be related to a larger
335 proportion of PUFA in QT0 compared to QT2 and QT4 (Fig. 8b). The determination of fatty
336 acid composition in fat bodies of queens allowed us to evaluate the levels of oxidative cell
337 damage. We calculated the relative peroxidability of membranes (peroxidation index, PI),
338 which decreased drastically from 29.5 at QT0, 7.9 at QT2 to 1.9 at QT4 (Fig. 8c).

339 Several hemolymph metabolites discriminate young queens, old queens and workers, in
340 agreement with results from fat body transcriptomics and highlight the importance of simple
341 sugars. Moreover, we observed that lipid concentrations in QT4 are consistent with the
342 upregulation of genes involved in the IIS pathway, *de novo* lipogenesis and with a
343 downregulation of *mdy* gene expression. Indeed, QT0 metabolism, as in FW, tends to facilitate
344 TG storage while the QT4 metabolism seems to be oriented towards the utilization of resources
345 for oogenesis without harmful lipid signatures.

346

347

DISCUSSION

Our results demonstrate that termite queens mobilize several mechanisms to sustain fertility and enable their remarkable lifespan without apparent costs of long-term massive reproduction. Against expectations, a gene coding an insulin-like peptide and components of the IIS pathway are upregulated in the fat body of highly fertile long-lived queens. The composition of lipids, the scarcity of stored fat observed in fat bodies of long-lived queens and the upregulated mitochondrial functions indicate that the energy metabolism required for reproduction remains efficient up to high age and does not require reserves to be stored in the queen's fat body.

Long lifespan on a carbohydrate diet

The intermediary metabolism in QT4 is centered on a high use of carbohydrates with an increase of glycolysis and the OXPHOS system for energy generation and the synthesis of specific lipids and proteins. The unexpected low trehalose concentration in long-lived queens, coupled with their high glucose levels also occurring in workers suggest that either trehalose is promptly hydrolyzed in physogastric queens or that glucose is an important component of what workers feed to physogastric queens in colonies with a well-developed fungus, without much trehalose synthesis in these queens. Poulsen *et al.*[43] have additionally shown that the diversity of decomposition enzymes encoded by the queen's microbiota is low and geared towards hydrolyzing simple sugars. Overall, all results confirm that long-lived queens receive a highly energetic feed enriched in simple sugars. In many organisms from *Drosophila* to humans, a prolonged carbohydrate-rich diet is associated with chronic metabolic diseases reducing lifespan[29,44]. Increased insulin secretion caused by such a diet leads to the accumulation of triglycerides, and disrupts IIS signaling over time leading to the development of insulin resistance[37,44,45]. In *M. natalensis* QT4, we were able to link the limited production of triglycerides from diglycerides to the non-canonical downregulation of a gene coding a

372 diacylglycerol acyltransferase (*mdy*), thus limiting a harmful accumulation of triglycerides in
373 the fat body.

374 *Antioxidant defense is strongest in young queens*

375 In young queens before mating (QT0), we observed an activation of the EGFR signaling
376 pathway and downstream signaling cascades that are known to coordinate multiple responses
377 such as the activation of apoptosis and remodeling (as described by Larsen[46], see also caste
378 determination in the honey bee[47]). After mating, three months pass before the appearance of
379 workers which feed all colony members. We observed that during the starvation period ending
380 at the QT1 stage, the absence of nutrition is associated with an upregulation of genes coding
381 for mitochondria biogenesis (OXPHOS system, mitochondrial ribosome subunits and transport)
382 and mitochondrial fission and degradation by autophagy. We also observed an upregulation of
383 the expression of genes coding for antioxidant enzymes which may suggest an increase of ROS
384 production. Several studies demonstrated that during calorie restriction, mitochondrial stress
385 induced by a transitory increase of ROS leads to a cellular adaptive response named
386 mitohormesis which allows an increase in stress resistance and promotes health and vitality[48].
387 We propose that a mitohermesis response occurs at the QT1 stage. Interestingly, gene
388 expression coding mitochondrial synthesis becomes upregulated again in mature queens, with
389 increased production in QT4 and at KT4 suggesting a maintenance of mitochondrial
390 biosynthesis which could be beneficial for health span. Associated with these results, we
391 observed a decrease of genes coding for antioxidant enzymes in reproductives. Similar results
392 were observed in honey bee[49] and ant[50] queens. These findings suggest that the mitochondria
393 of long-lived reproductives remain efficient and produce a comparatively low amount of ROS,
394 thus limiting oxidative damage, one of the main drivers of aging.

395

396

Surprising upregulation of IIS pathway components

We observed several modifications, potentially triggered by social nutrition at the QT2 stage. We observed a first upregulation of the *vg* gene. As recently suggested for other termite species[39], polyploidy in the fat body of *M. natalensis* queens can boost their egg production by increasing protein synthesis, notably VG. In *Drosophila*, seven out of eight insulin-like peptides (DILPs) are mainly produced in the brain insulin-producing cells except for DILP6, which is produced in the fat body. *dIlp6* gene expression is up-regulated during starvation[51,52]. In the social bee, *Apis mellifera*, two *Ilp* genes coding AmILP1 and AmILP2 are expressed in both tissues[53]. In *M. natalensis*, we identified only two genes from separate loci coding an ortholog to DILP7 (not expressed in *M. natalensis* fat bodies) and a further paralog found across holo- and hemimetabolous insects, without a clear ortholog in *Drosophila melanogaster*, which we called *Ilp9* (Supplementary Fig. 5). During queen maturation, we observed potential increases in insulin suggested by upregulated expression of *Ilp9*. If this occurs in long-lived queens in response to increases in some carbohydrates, then this would be reminiscent of processes in mammalian pancreatic beta-cells[54]. Not only does the expression of *Ilp9* increase concomitantly with the formation of the royal fat body, it is also approximately 800-fold more expressed in fat bodies of reproductives compared to workers. The increase of *Ilp9* gene expression was not associated with an activation of TORC1, although the expression of genes involved in protein synthesis were upregulated in the fat body of reproductives. However, we observed an increase of *elF6* gene expression which is involved in insulin-stimulated translation, most notably controlling adipogenic transcription factors like *crc* (also known as *ATF4*), a member of the mTOR-independent pathway[35,55]. We propose that the IIS pathway, including the *Ilp9* gene, activates the eIF6-*crc* gene program in the fat body of mature queens and kings. This in turn increases the synthesis of proteins involved in lipid synthesis and essential for fecundity, despite a downregulation of the TORC1 signaling pathway elsewhere described as the main pathway

422 for protein synthesis[56] and also downregulated in whole bodies of reproductives of lower
423 termite species[21,22].

424

425 *No damaging fat signatures and no fat storage in long-lived queens*

426 Simultaneously with the gradual establishment of the pattern of IIS signaling, we observed a
427 gradual upregulation of *de novo* lipogenic genes. Calculations based on lipid compositions in
428 fat bodies of queens of different ages highlighted significant changes in the proportion of
429 PUFA/MUFA/SFA with a decrease of PUFA concentrations. PUFA are a thousand times more
430 likely to oxidize than MUFA[57]. The oxidation of PUFA can set off an oxidative cascade with
431 the formation of radicals capable of damaging surrounding macromolecules and tissues[57].
432 Therefore, this decrease in PUFA concentrations can lead to a reduction in oxidative damage
433 and thus increase lifespan of queens. In agreement with this, we found a strong, progressive
434 decline of the peroxidation index (PI) indicating resistance of membranes to peroxidative
435 damage. Several studies in mammals, birds and invertebrates[57,58] have demonstrated that PI
436 values inversely correlate with longevity. In honey bees, queens also have a lower PI than
437 female workers[57]. Moreover, gradually downregulated expression of the *mdy* gene, coding a
438 diacylglycerol acyltransferase enzyme catalysing the final step of TG synthesis from DG[59],
439 corroborates the decrease of TG concentrations we observed during adult queen maturation
440 suggesting very limited storage of lipids in favor of immediate utilization. Also, we observed a
441 trend for DG to increase, which are known to be preferably used for lipid transport (not free
442 fatty acid as in vertebrates)[60]. Han & Bordereau already observed almost forty years ago by
443 electronic microscopy that lipid droplet number decreases during *Macrotermes* termite queen
444 maturation[38]. The decrease of *mdy* gene expression was also observed in the fat body of mature
445 kings, suggesting that the low level of stored TG can be generally beneficial for long-lifespan
446 in reproductives and is not just explaining the absence of a cost of reproduction in queens. This

447 suggests that the gene network involving *mdy* would be a target for research linked to the
448 accumulation of excess fat.

449 Although further investigations of, for example, kings of different ages and also
450 functional studies are necessary, our unique analysis reveals a remodeling of the fat body during
451 adult queen maturation concomitantly with changes in nutritional and social conditions. The
452 results suggest that the IIS signaling network may have been adapted in queen fat bodies to
453 maintain high fertility while also enabling their remarkable lifespan. Together with the
454 composition of lipids and the scarcity of stored fat observed, this seems to optimize both
455 sustained fecundity and health span, avoiding hyperfunction[61] and defying the trade-off
456 between reproduction and survival. Finally, we observed several upregulated cellular functions
457 in mature reproductives that are otherwise known to decline with age, notably mitochondrial
458 functions and DNA damage repair. Altogether, our findings on the aging process of *M.*
459 *natalensis* highlight potential molecular targets which could be involved in age-related
460 metabolic diseases in humans.
461

462 **METHODS**

463 **Species studied**

464 The termite *Macrotermes natalensis* (Haviland, 1898) belongs to the Macrotermitinae
465 (Termitidae, Blattodea), the only subfamily that has established an exo-symbiotic obligatory
466 relationship with basidiomycete fungi of the genus *Termitomyces*[62]. It lives in large colonies in
467 Southern Africa where it builds massive mounds[63]. When the colony is mature and in
468 appropriate environmental conditions, winged male and female imagoes leave the mound
469 during spring and disperse in synchronous swarms across colonies[64]. Male imagoes locate
470 female imagoes[65] and after pairing, couples perform dealation and establish new colonies as

queen and king[64]. They mate throughout their life and fertilize all eggs. Few months after the establishment of the colony, workers explore the environment to collect spores and to inoculate the fungus comb they build in the nest[66]. During the first years larvae emerge which become sterile workers or soldiers[67]. Minor workers and soldiers are female and major workers are male[68]. Mature colonies contain around one million short-lived sterile individuals. Workers feed all colony members through trophallaxis (transfer of food from mouth to mouth), after a complex digestion of lignocellulose by the fungus and intestinal microbiota[43]. The royal couple lives for more than 20 years in a royal cell[11,69]. The old queen lays thousands of eggs per day[14] while the median lifespan of a worker is 56 days[12,33]. After five to seven years, some larvae develop into nymphs which become imagoes after several instars.

Sampling

Field colonies opened to collect animals had been followed for over 20 years by Jannette Mitchell in a field belonging to the University of Pretoria (coordinates in Supplementary Table 8)[64]. Old minor workers (FW) and 20-year old queens (QT4) and kings (KT4) were sampled from at least twenty-year-old colonies. Less than an hour was taken to reach the royal cells containing QT4 and KT4. We observed that habitacle volumes were comparable between colonies (data not shown), suggesting that the colonies were of the same age. QT4 and KT4 also showed limited variability in weight and length between colonies.

Establishment and maintenance of incipient termite colonies

Imagoes were collected in Pretoria (South Africa) in 2016 and 2018 during the spring swarming flights (coordinates in supplementary Table 8). Mounds were covered with nets to retrieve imagoes. These were placed in large boxes preserving humidity and immediately transferred to the laboratory. Individuals were sexed by visual observation of their abdominal sternites, weight and length were recorded and wings were manually removed. Establishment of

laboratory incipient colonies occurred for both field trips, following a protocol adapted from Lepage[32] and Han & Bordereau[33] (and Supplementary Fig. 6). In October 2016 and 2018, imagoes were collected from five colonies each time (males from a single colony, females twice from four different ones). Per colony providing females (eight in total), 200 incipient colonies were established. Each paired couple was introduced in a closed plastic box (6 x 5 x 4.5 cm) filled with sieved soil collected near the mounds. The incipient colonies were kept in a breeding room with controlled conditions: 28°C, 85% relative humidity and 12:12 photoperiod. Water was used to keep the soil slightly moistened. Development of the colonies was visually monitored. At three months, when workers started to explore, small pieces of dry wild oats were supplied on the surface of the soil and wood was additionally supplied after 4.5 months. A *Termitomyces sp.* fungus comb with nodules was collected from one mature field colony and a small part of this comb was introduced in each box. After 3.5 months, mortality was 56% for the 2016 incipient colonies (± 15% across field colonies of origin) and 30 ± 7% for the 2018 incipient colonies. When the termite populations outgrew their boxes, they were opened on one side and placed inside bigger ones (18 x 12 x 7.5 cm after 3 months, 36 x 24 x 14 cm after 14 months, and 1000 x 70 x 40 cm after 21 months) filled with sieved moistened soil. Colonies were checked every two days to supply water and food if needed and to remove moldy food. Queens were sampled after 3 months (QT1) and 9 months (QT2) in colonies established from both trips, and after 31 months (QT3) for the 2016 mission. At QT1, the number of minor and major workers, soldiers, presoldiers, and larvae were counted in colonies where queens were sampled. At QT2, these were also counted and weight of the fungus measured.

Species identity

Total DNA was isolated from the head and the legs of one imago of each of the 9 colonies. PCR was performed using the cytochrome oxidase I gene primers: LCO 5'- GGT CAA CAA ATC ATA AAG ATA TTG G -3' and HCO 5'- TAA ACT TCA GGG TGA CCA AAA AAT CA -

3'[70] and the 650-bp amplified fragment was sequenced and analyzed using the Barcode of Life Database identification system (www.barcodinglife.org). Species identity of each colony was confirmed to be *M. natalensis*[43].

Hemolymph and fat body collection

Hemolymph and fat body were collected from cold-anesthetized individuals (FW, QT0, QT1, QT2, QT3 and QT4). A total of 85 FW were pooled in one hemolymph and fat body sample while ten QT1, QT2 or QT3 were pooled. We obtained eight samples except for QT3 (three samples). Hemolymph was collected under a binocular microscope with tapered glass Pasteur pipettes inserted in the membranous part just behind the head. The mean volume of hemolymph collected per individual was 0.5 µL for FW, 1.5 µL for QT0, QT1, QT2, 50 µL for QT3, and 1 mL for QT4. Hemolymph samples were collected in cryotubes, quickly frozen in liquid nitrogen and kept at -80°C until use.

Subsequently, termites were killed by decapitation and abdominal fat body was collected. For RNA and DNA extraction, the fat body was stored in a tube containing RNAlater buffer (Invitrogen) and kept at -80°C until use. For lipid and metabolite analyses, nitrogen-frozen fat bodies were crushed in a tube which was immediately frozen in liquid nitrogen and kept at -80°C until use. For ploidy analyses, fat body was collected from one individual, stored in a tube containing 200 µL of Cycletest PLUS DNA Reagent Kit buffer (Becton Dickinson) and kept at -80°C until use.

RNA profiling

In the 2016 cohort (4 FW, 4 QT0, 4 QT1, 1 QT2, 3 QT3, 4 QT4 and 3 KT4) and 2018 cohort (2 QT2), total RNA was isolated from fat body samples using miRNeasy Micro kit (Qiagen) and RNAse-free DNAse according to the manufacturer's instructions (Qiagen). RNA-Seq library preparations were carried out from 500 ng total RNA using the TruSeq Stranded mRNA kit (Illumina, San Diego, CA, USA) which allows mRNA strand orientation (sequence reads occur in the same orientation as anti-sense RNA). Briefly, poly(A)$^+$ RNA was selected with oligo(dT) beads, chemically fragmented and converted into single-stranded cDNA using random hexamer priming. Then, the second strand was generated to create double-stranded cDNA. cDNA were 3'-adenylated and Illumina adapters added. Ligation products were PCR-amplified. All libraries were subjected to size profile analysis conducted by Agilent 2100 Bioanalyzer (Agilent Technologies, Santa Clara, CA, USA) and qPCR quantification (MxPro, Agilent Technologies, Santa Clara, CA, USA) using the KAPA Library Quantification Kit for Illumina Libraries (KapaBiosystems, Wilmington, MA, USA), then sequenced using 150 bp paired end reads chemistry on a HiSeq 4000 Illumina sequencer (Illumina, San Diego, CA, USA). An Illumina filter was applied to remove the least reliable data from the analysis. The raw data were filtered to remove any clusters with too much intensity corresponding to bases other than the called base. Adapters and primers were removed on the whole read and low-quality nucleotides were trimmed from both ends (when quality value was lower than 20). Sequences between the second unknown nucleotide (N) and the end of the read were also removed.

RNA-seq analyses

RNAseq reads were mapped against the *M. natalensis* genome[43] using *hisat2* (version 2.1.0[71]) at default settings. Gene expression levels were then generated by counting reads mapping to

each gene of the *M. natalensis* genome (annotation version 2.3) using *htseq-count*[72]. Differential expression analyses were carried out in R (3.5.1) with the DESeq2 package[73], comparing between all pairs of castes and queen stages, as well as comparing each caste and queen stage against all others. Genes were considered significantly differentially expressed if the adjusted *p*-value was less than 0.05. Principal component analyses (PCA) were also carried out within the DESeq2 package[73]. Counts were transformed using the *varianceStabilizingTransformation* function, and the PCA was calculated and plotted using the *plotPCA* function. This function carries out a PCA on the top 500 genes, based on variance. A weighted gene co-expression network (WGCN) was generated with these gene expression counts, using the R package WGCNA[34]. Normalized counts were extracted from the DESeq2 data set with the *counts* function. These data were filtered for genes with zero variance or with missing values with the WGCNA function *goodSamplesGenes.* With the remaining 9631 genes, a signed WGCN was created using a soft power of 14, implementing the biweight midcorrelation calculation and setting the minimum module size to 30. Modules with a dissimilarity less than 0.5 were merged using the *mergeCloseModules* function. We related the expression profiles of the resulting nine modules to castes and queen stages by correlating (Pearson's *r*) the module eigengenes (first principal component of the expression matrix of each module) with a binary vector, containing 0s and 1s depending on the membership of each sample (FW, QT0, QT1, QT2, QT3, QT4 or KT4). A significant positive correlation signifies an overall upregulation while a negative correlation signifies a downregulation of expression within the module for a given caste or queen stage.

To visualize the WGCN, we first reduced the WGCN to include only the most highly connected nodes. We did this by retaining genes with a topological overlap of at least 0.2 with at least another gene, and by including the top 15 most connected genes within each module. This reduced WGCN (5823 genes) was exported to Cytoscape (version 3.8.0[74]) with the

591 *exportNetworkToCytoscape* function in WGCNA (threshold 0.15). In Cytoscape, the network
592 was rendered using the Edge-weighted Spring Embedded Layout and nodes were colored by
593 module membership or expression fold change. GO term enrichment analyses were carried out
594 with topGO (version 2.34.0[75]), using the classic algorithm. Node size was set to 5, Fisher exact
595 tests were applied, and we only kept GO terms that matched with 2 genes at least and with a *p*-
596 value < 0.05.

597

598 **Analysis of ILPs**

599 Two ILP genes (Mnat_00258 and Mnat_03820) were found in the *M. natalensis* proteome
600 based on orthology to ILPs in *D. melanogaster*. Orthology groups had been determined in a
601 previous study [76] using orthoMCL [77]. We checked for further ILP genes within the genome by
602 mapping the protein sequences of these two *M. natalensis* genes and eight known *D.*
603 *melanogaster* ILPs (downloaded from NCBI; accessed February 2021) against the *M.*
604 *natalensis* genome. This was carried out with exonerate (v 2.2.0 [78]) using the protein2genome
605 model at default settings. No further ILP copies were found but the annotations of the two *M.*
606 *natalensis* genes were improved based on these exonerate alignments. ILP protein sequences
607 from 16 further insects (*Aedes aegypti, Apis mellifera, Atta cephalotes, Acromyrmex echinatior,*
608 *Blattella germanica, Camponotus floridanus, Cryptotermes secundus, Ephemera Danica,*
609 *Harpegnathos saltator Linepithema humile, Nasonia vitripennis, Pogonomyrmex barbatus,*
610 *Rhodnius prolixus, Solenopsis invicta, Tribolium castaneum, Zootermopsis nevadensis* and
611 *Strigamia maritima)* were extracted from the same orthology database and aligned with the *M.*
612 *natalensis* and *D. melanogaster* sequences using MAFFT (v7.397 [79]) with the E-INS-I strategy.
613 A gene tree was constructed with FastTree (v. 2.1.10 [80]) and visualized with iTOL[81].

614

615

Metabolomic analysis

A volume of 20 µL of hemolymph (from 2016 and 2018 experiments; 6 FW, 8 QT0, 7 QT1, 7 QT2, 3 QT3 and 4 QT4 samples) was used to determine metabolic profiles obtained by gas chromatography coupled with mass spectrometry (GC-MS). We used the experimental procedure described in Khodayari *et al.*[82], and adapted in Genitoni *et al.*[83]. Samples were homogenized in 450 µL of ice-cold methanol/chloroform (2:1, v/v) before the addition of 300 µL of ultra-pure water. After they have been vigorously vortexed, the samples were centrifuged for 10 min at 4,000 g (4°C). Then, 100 µL of the upper phase, which contains metabolites, was transferred to new glass vials (Thermofisher), speedvac dried at RT, and vials sealed with PTFE caps. The derivatization of the samples was conducted with a CTC CombiPAL autosampler (CTC Analytics AG, Zwingen, Switzerland), as described in Khodayari *et al.*[82]. The GC-MS platform consisted of an Agilent 7890B gas chromatograph coupled to a 5977B mass spectrometer. The injector was held at 250°C, and the temperature of the oven ranged from 70 to 170°C at 5°C/min, from 170 to 280°C at 7°C/min, and from 280 to 320°C at 15°C/min; at the end of the temperature ramps, the oven remained at 320°C for 4 min. A 30 m fused silica column (HP5 MS 30 m, I.D. 0.25 mm, thickness 0.25 µm, 5% Diphenyl / 95% dimethylpolysiloxane, Agilent Technologies) was used with helium as the gas carrier at 1 mL per min. The temperatures of the transfer line and ion source were 280 and 230°C, respectively. The split mode (split ratio: 2:1) was used for the injection of 1 µL of each sample, and detection was realized by electronic impact (electron energy: 70 eV) in full scan mode. The peaks list was annotated based on their MS fragmentation patterns with MassHunter. Detected metabolites were identified, and calibration curves were used to calculate the concentration of each metabolite.

Statistical analysis

Permutational MANOVA[84] was used to test for differences in multivariate metabolite concentrations between stages and castes. We subsequently tested for differences in individual metabolites between pairs of subsequent stages or between FW vs. QT0 and FW vs. QT4. The concentrations of all metabolites were log transformed and compared between groups by using Welch tests. Tail probabilities were corrected for multiple testing using the Benjamini-Hochberg method. Tests were considered significant for a p-value < 0.05 and carried out using R software (v 3.6.3).

Lipidomic analysis

Lipids were extracted for fatty acid profile analysis gas chromatography with flame ionization detection (GC-FID) and gas chromatography coupled to mass spectrometry (GC-MS). Lipidomic analyses were done by liquid chromatography coupled to mass spectrometry (LC-HRMS/MS). Lipids were extracted from 20 µL of hemolymph (from 4 FW and 4 QT4) or from fat body (from 4 QT0, 3 QT2 and 3 QT4) using a biphasic solvent system of cold methanol, methyl tert-butyl ether (MTBE), and water, adapted from Cajka *et al.*[85]. Briefly, the samples were transferred in 750 µL of MTBE and 150 µL of methanol into a 2 mL screw cap tube. For lipidomic analysis, 1µL of internal standard (PC 31: 1|PC17:0-PC14:1) at 3,775 µg/mL was added to each sample. After homogenization with the "Precellys tissue homogenizer" at 5,000 rpm for 5 minutes, 400 µL of H_2O was added to each sample. The samples were then centrifuged at 13,000 rpm for 5 min. The upper phase containing the lipids (MTBE) was transferred into a new tube and dried under a stream of nitrogen at 20°C. For fatty acid profile analysis, extracted lipids were transferred in 100 µL of MTBE, methylated into fatty acids of methyl esters (FAMEs) after the addition of 10 µL of tetramethylammonium hydroxide (TMAH). After a centrifugation at 4,000 rpm during 5 min, supernatants were collected and

664 diluted 3 times into heptane prior to injection into GC-FID and GC-MS. For lipidomic analysis,
665 lipids extracted were taken up into 100 µL of isopropanol before injection into LC-HRMS/MS.

666 *FAMEs analysis*

667 Fatty acid profiles were separated and analyzed by a gas chromatography with flame ionization
668 detection (GC-FID 2010 Plus Shimadzu) equipped with a BPX 70 capillary column (SGE,
669 30 m × 0.25 mm, 0.25 µm) as described in Merlier *et al.*[86]. The fatty acids were identified by
670 comparison of the retention times of a standard solution of 37 fatty acid methyl esters (Sigma;
671 47885-U Supelco) in GC-FID and confirmed by high accuracy mass of molecular ions and their
672 fragments after injection into a GC-MS (Q-Exactive™, Thermo)[86]. The composition of fatty
673 acids was expressed as a relative percentage of their peak areas with respect to the total peak
674 area of all the fatty acids. The fat body samples were normalized by dividing peak areas with
675 total DNA concentration (ng/mL) measured with a Qubit Fluorometer (Thermofisher) and
676 Qubit dsDNA Assay kit (Invitrogen). The membrane peroxidation index (PI) of lipid extracts
677 in fat bodies of queens was calculated as the sum of bis-allylic methylene groups per 100 fatty
678 acids according to the equation[57] :

679 PI=(percentage of dienoics x 1) + (percentage of trienoics x 2) + (percentage of hexaenoics x 5)

680 *Untargeted lipidomics analysis*

681 The untargeted lipidomics analysis was conducted using a liquid chromatography-high
682 resolution tandem mass spectrometry (LC-HRMS/MS) analysis used as described and modified
683 from Ulmer *et al.*[87]. An HPLC 1290 (Agilent Technologies) coupled to a hybrid quadrupole
684 time-of-flight high definition (QtoF) mass spectrometer Agilent 6538 (Agilent Technologies)
685 equipped with an ESI dual source was used. Lipids were separated on a C18 Hypersil Gold
686 (100 x 2.1 mm, 1.9 µm, Thermofisher) at 50°C, using an elution gradient composed of a solution
687 of 20 mM of ammonium acetate and 0.1% formic acid (ACN: H_2O, 60:40, v/v) (solvent A) and

a solution of 20 mM of ammonium acetate and 0.1% formic acid (IPA: ACN:H_20, 90:8:2, v/v) (solvent B). Separation was conducted under the following gradient: 0–2 min from 32% (B), 2–3 min from 32% to 40% (B), 3–8 min from 40% to 45% (B), 8–10 min from 45% to 50% (B), 10–16 min from 50% to 60% (B), 16–22 min from 60% to 70% (B), 22–28 min from 70% to 80% (B), 28–30 min from 80% to 99% (B), 30–31 min from 99% to 32% (B), 31–36 min from 32% to 32% (B). The flow rate was set at 250 µL/min. Two µL of samples were injected. MS / MS spectra were acquired in positive mode and in negative mode in data dependent and MS^2 scans were performed on the sixth most intense ions. The source temperature, fragmentor and the skimmer were set up at 350°C, 150 V and 65 V, respectively. The acquisition was made in full scan mode between 100 m/z and 1700 m/z, with a scan of two spectra per second. Two internal references were used for in-run calibration of the mass spectrometer (121.0509, 922.0098 in positive ion mode and 112.9856, 1033.9881 in negative ion mode). MassHunter B.07 software allowed us to control the parameters of the machine acquired.

Data processing and annotation

MsDial v4.0 software[88] was used for data processing and annotation of lipids. The data collection was performed by fixing the MS1 and MS2 tolerance, at 0.01 Da and 0.025 Da, respectively. The peak detection was fixed at 1000 amplitude and a mass slice width at 0.1 Da. The deconvolution parameters correspond to a sigma window value at 0.5 and a MS/MS abundance cut off at 10 amplitude. Isotopic ions were kept until 0.5 Da. The peaks list was annotated based on their unique MS/MS fragmentation patterns using the in-built LipidBlast mass spectral library in MS-DIAL software. The accurate mass tolerance MS1 and MS2 were fixed -at 0.01 Da and 0.05 Da respectively. The identification score cut off was fixed at 80%. Lipids were normalized by the intensity of the internal standard (PC 31: 1|PC17:0-PC14:1).

Statistical analysis for lipidomic data

Permutational MANOVA[84] on ilr-transformed compositional data[89] was used to test for differences in SFA, MUFA and PUFA lipid content in hemolymph of FW and QT4. Similarly, to compare the percentages of SFA, MUFA, PUFA lipid content in fat bodies of different queen stages we used a permutational MANOVA followed by pairwise post-hoc perMANOVA comparisons of each stage with QT4 (Holm-Bonferroni correction for multiple comparisons). To compare log-transformed individual lipid values between FW and QT4, or between QT0, QT2 and QT4, Welch tests were used, corrected for multiple testing using the Benjamini-Hochberg method. To compare the peroxidation index (PI) in fat bodies of different queen stages we used Kruskal-Wallis test followed by Dunn's post hoc comparisons. All tests were considered significant for a p-value < 0.05 and were carried out using R software (v 4.0.2). Heatmaps were made using the heatmap function in the Metaboanalyst v 4.0. with Euclidean distance and clustering using Ward's method.

Ploidy analysis

Fat body from 2016 and 2018 cohort samples (4 QT0, 4 QT1, 3 QT2, 3 QT3 and 6 QT4) was processed by Flow Cytometric Analysis with a Cycletest PLUS DNA Reagent Kit (BD Biosciences, Le pont de Claix). All procedures were adapted from Nozaki & Matsuura[39]. Stained nuclei were analyzed for DNA-PI fluorescence using an Accuri C6 Flow Cytometer (BD Biosciences) at an excitation wavelength of 488 nm and a detector equipped with an 585/45 bandpass filter. Approximately 1,000 cells were acquired for each measurement. Flow cytometric analyses were performed with the Accuri C6 software v1.0.264.21 (BD Biosciences). Debris were removed on an FSC-A/SSC-A dotplot and doublet were eliminated with and PI-FL2-H/ FL2-A dot plot. The nuclei were analyzed with a histogram PI-A. The 1C

736 DNA peak was determined by the analysis of king's testis (sperm), allowing the identification
737 of the 2C, 4C, and 8C peaks of the others samples.

738 *Statistical analysis for ploidy*

739 To compare percentages of nuclei with different multiples of haploid genomes between queen
740 stages, we used permutational MANOVA followed by pairwise post-hoc perMANOVA (Holm-
741 Bonferroni correction for multiple comparisons).

742

743 **Acknowledgements**

744 The authors would like to thank Dr Christian Bordereau and Dr Jannette Mitchell for helpful
745 discussions on the termite model. The authors acknowledge the Department of Public Works
746 and Infrastructure, Pretoria and the University of Pretoria for allowing access to their sites of
747 collect of *M. natalensis*. The authors also thank Cyril Fresillon and Pierre Deparscau,
748 photographers for the CNRS images. We thank Qi Li for termite colony maintenance. This
749 study was supported by the International Human Frontier Science Program RGP0060/2018 to
750 M.V.C. S.S was also supported by a fellowship from Université de Paris Est-Créteil (UPEC).
751 A.L. acknowledges financial support from France Génomique (ANR-10-INBS-09-08). We
752 would like to thank the EcoChim platform of University of Rennes for access to metabolomics
753 facilities.

754

755 **Author contributions**

756 M.V.C designed the study. D.S-D., A.R., R.L., L-A.P., Z.W.D.B., and M.V.C. carried out
757 termite experiments, M.V.C and A.L. transcriptomic, D.R. and R.L. metabolomic and S.A. and
758 R.L. lipidomic experiments. M.A. and M.V.C. measured DNA contents. S.S., M.H., T.V.D

759 and M.V.C. analyzed the data, wrote the original draft and were responsible for the figures and
760 tables presented. All authors contributed with expertise, input, and edits throughout the text.
761

762 **Competing interests**

763 The authors declare that they have no conflict of interest.

764

765 **Data availability**

766 The authors declare that all data supporting the findings of this study are available within the
767 paper and supplementary information files, or are available from a dedicated github repository:
768 https://github.com/MCH74/Mnat_analyses. RNA-seq reads generated in this study are
769 available in Sequence Read Archive (BioProject ID: PRJNA685589 and BioSample
770 accessions: SAMN17088123- SAMN17088147).
771

772 **Additional informations**

773 Supplementary Information accompanies this paper.
774

775 **REFERENCES**

776 1. Johnson, A. A. & Stolzing, A. The role of lipid metabolism in aging, lifespan regulation,
777 and age-related disease. *Aging Cell* **18**, e13048 (2019).
778 2. Balaban, R. S., Nemoto, S. & Finkel, T. Mitochondria, oxidants, and aging. *Cell* **120**,
779 483–495 (2005).
780 3. Flatt, T. Survival costs of reproduction in *Drosophila*. *Experimental Gerontology* **46**,
781 369–375 (2011).
782 4. Kirkwood, T. B. L. Evolution of ageing. *Nature* **270**, 301–304 (1977).
783 5. Kirkwood, T. B. L. & Austad, S. N. Why do we age? *Nature* **408**, 233–238 (2000).
784 6. Maklakov, A. A. *et al.* Antagonistically pleiotropic allele increases lifespan and late-life
785 reproduction at the cost of early-life reproduction and individual fitness. *Proceedings of*
786 *the Royal Society B: Biological Sciences* **284**, 20170376 (2017).
787 7. Williams, G. C. Natural Selection, the Costs of Reproduction, and a Refinement of
788 Lack's Principle. *The American Naturalist* **100**, 687–690 (1966).
789 8. Edward, D. A. & Chapman, T. Mechanisms underlying reproductive trade-offs: Costs
790 of reproduction. *Mechanisms of Life History Evolution* (Oxford University Press, 2011).
791 9. Hansen, M., Flatt, T. & Aguilaniu, H. Reproduction, fat metabolism, and life span: What
792 Is the Connection? *Cell Metabolism* **17**, 10–19 (2013).
793 10. Taormina, G. *et al.* Longevity: Lesson from model organisms. *Genes* **10**, 518 (2019).
794 11. Carey, J. R. Demographic mechanisms for the evolution of long life in social insects.
795 *Experimental Gerontology* **36**, 713–722 (2001).
796 12. Traniello, J. F. A. & Leuthold, R. H. Behavior and ecology of foraging in termites. In
797 *Termites: Evolution, Sociality, Symbioses, Ecology* (eds. Abe, T., Bignell, D. E. &
798 Higashi, M.) 141–168 (Springer Netherlands, 2000).
799 13. Keller, L. & Genoud, M. Extraordinary lifespans in ants: a test of evolutionary theories
800 of ageing. *Nature* **389**, 958–960 (1997).
801 14. Kaib, M., Hacker, M. & Brandl, R. Egg-laying in monogynous and polygynous colonies
802 of the termite *Macrotermes michaelseni* (Isoptera, Macrotermitidae). *Insectes soc* **48**,
803 231–237 (2001).
804 15. Kuhn, J. M. M., Meusemann, K. & Korb, J. Disentangling the aging network of a termite
805 queen. Preprint at https://www.biorxiv.org/content/10.1101/2020.12.19.423576v1
806 (2020).
807 16. Rodrigues, M. A. & Flatt, T. Endocrine uncoupling of the trade-off between
808 reproduction and somatic maintenance in eusocial insects. *Current Opinion in Insect*
809 *Science* **16**, 1–8 (2016).
810 17. von Wyschetzki, K., Rueppell, O., Oettler, J. & Heinze, J. Transcriptomic signatures
811 mirror the lack of the fecundity/longevity trade-off in ant queens. *Molecular Biology*
812 *and Evolution* **32**, 3173–3185 (2015).
813 18. Heinze, J. & Schrempf, A. Aging and reproduction in social insects – A Mini-Review.
814 *GER* **54**, 160–167 (2008).
815 19. Harrison, M. C. *et al.* Gene co-expression network reveals highly conserved, well-
816 regulated anti-ageing mechanisms in old ant queens. *Genome Biology and Evolution*
817 (2021).
818 20. Korb, J. *et al.* Comparative transcriptomic analysis of the mechanisms underpinning
819 ageing and fecundity in social insects. *Philosophical Transactions of the Royal Society*
820 *B: Biological Sciences* **376**, 20190728 (2021).
821 21. Lin, S., Werle, J. & Korb, J. Transcriptomic analyses of the termite, *Cryptotermes*
822 *secundus*, reveal a gene network underlying a long lifespan and high fecundity.
823 *Communications Biology* **4**, 1–12 (2021).

824 22. Haroon *et al.* Transcriptomic evidence that insulin signalling pathway regulates the
825 ageing of subterranean termite castes. *Scientific Reports* **10**, 8187 (2020).
826 23. Pan, H. & Finkel, T. Key proteins and pathways that regulate lifespan. *Journal of*
827 *Biological Chemistry* **292**, 6452–6460 (2017).
828 24. Teleman, A. A. Molecular mechanisms of metabolic regulation by insulin in
829 *Drosophila*. *Biochemical Journal* **425**, 13–26 (2009).
830 25. Bjedov, I. *et al.* Mechanisms of life span extension by rapamycin in the fruit fly
831 *Drosophila melanogaster. Cell Metabolism* **11**, 35–46 (2010).
832 26. Partridge, L., Alic, N., Bjedov, I. & Piper, M. D. W. Ageing in *Drosophila*: the role of
833 the insulin/Igf and TOR signalling network. *Experimental Gerontology* **46**, 376–381
834 (2011).
835 27. Giannakou, M. E. *et al.* Long-lived *Drosophila* with overexpressed dFOXO in adult fat
836 body. *Science* **305**, 361–361 (2004).
837 28. Fontana, L. & Partridge, L. Promoting health and longevity through diet: from model
838 organisms to humans. *Cell* **161**, 106–118 (2015).
839 29. Álvarez-Rendón, J. P., Salceda, R. & Riesgo-Escovar, J. R. *Drosophila melanogaster*
840 as a model for diabetes type 2 progression. *BioMed Research International* vol. 2018
841 (2018).
842 30. Arrese, E. L. & Soulages, J. L. Insect fat body: energy, metabolism, and regulation.
843 *Annu. Rev. Entomol.* **55**, 207–225 (2009).
844 31. Li, S., Yu, X. & Feng, Q. Fat body biology in the last decade. *Annual Review of*
845 *Entomology* **64**, 315–333 (2019).
846 32. Lepage, M. Development in the laboratory of incipient colonies of *Macrotermes*
847 *michaelseni* (Sjoestedt) (Isoptera, Macrotermitidae). *Annales de la Societe*
848 *Entomologique de France* (1990).
849 33. Han, S. H. (Universite d'Abidjan & Bordereau, C. From colony foundation to dispersal
850 flight in a higher fungus-growing termite, *Macrotermes subhyalinus*, (Isoptera,
851 Macrotermitinae). *Sociobiology (USA)* (1992).
852 34. Langfelder, P. & Horvath, S. WGCNA: an R package for weighted correlation network
853 analysis. *BMC Bioinformatics* **9**, 559 (2008).
854 35. Brina, D. *et al.* eIF6 coordinates insulin sensitivity and lipid metabolism by coupling
855 translation to transcription. *Nature Communications* **6**, 8261 (2015).
856 36. Buszczak, M., Lu, X., Segraves, W. A., Chang, T. Y. & Cooley, L. Mutations in the
857 *midway* gene disrupt a Drosophila Acyl Coenzyme A: Diacylglycerol Acyltransferase.
858 *Genetics* **160**, 1511–1518 (2002).
859 37. Wang, Y., Viscarra, J., Kim, S.-J. & Sul, H. S. Transcriptional regulation of hepatic
860 lipogenesis. *Nature Reviews Molecular Cell Biology* **16**, 678–689 (2015).
861 38. Han, S. H. & Bordereau, C. Origin and formation of the royal fat body of the higher
862 termite queens. *J. Morphol.* **173**, 17–28 (1982).
863 39. Nozaki, T. & Matsuura, K. Evolutionary relationship of fat body endoreduplication and
864 queen fecundity in termites. *Ecology and Evolution* **9**, 11684–11694 (2019).
865 40. Herzig, S. & Shaw, R. J. AMPK: guardian of metabolism and mitochondrial
866 homeostasis. *Nature Reviews Molecular Cell Biology* **19**, 121–135 (2018).
867 41. Jeon, S.-M. Regulation and function of AMPK in physiology and diseases. *Exp Mol*
868 *Med* **48**, e245 (2016).
869 42. Thompson, S. N.. Trehalose—the insect 'blood'sugar. *Advances in insect*
870 *physiology*, Vol *31*, 205-285. (Elsevier, 2003).
871 43. Poulsen, M. *et al.* Complementary symbiont contributions to plant decomposition in a
872 fungus-farming termite. *PNAS* **111**, 14500–14505 (2014).
873 44. Lee, D., Son, H. G., Jung, Y. & Lee, S.-J. V. The role of dietary carbohydrates in

organismal aging. *Cellular and Molecular Life Sciences* **74**, 1793–1803 (2017).
45. Musselman, L. P. *et al.* A high-sugar diet produces obesity and insulin resistance in wild-type *Drosophila*. *Disease Models & Mechanisms* **4**, 842–849 (2011).
46. Larsen, W. J. Cell remodeling in the fat body of an insect. *Tissue and Cell* **8**, 73–92 (1976).
47. Kamakura, M. Royalactin induces queen differentiation in honeybees. *Nature* **473**, 478–483 (2011).
48. Ristow, M. & Schmeisser, K. Mitohormesis: Promoting health and lifespan by increased levels of reactive oxygen species (ROS). *Dose-Response* **12**, dose-response.13-035.Ristow (2014).
49. Corona, M., Hughes, K. A., Weaver, D. B. & Robinson, G. E. Gene expression patterns associated with queen honey bee longevity. *Mechanisms of Ageing and Development* **126**, 1230–1238 (2005).
50. Parker, J. D., Parker, K. M., Sohal, B. H., Sohal, R. S. & Keller, L. Decreased expression of Cu–Zn superoxide dismutase 1 in ants with extreme lifespan. *PNAS* **101**, 3486–3489 (2004).
51. Slaidina, M., Delanoue, R., Gronke, S., Partridge, L. & Léopold, P. A *Drosophila Insulin-like Peptide* Promotes Growth during Nonfeeding States. *Developmental Cell* **17**, 874–884 (2009).
52. Bai, H., Kang, P. & Tatar, M. *Drosophila insulin-like peptide-6* (*dilp6*) expression from fat body extends lifespan and represses secretion of *Drosophila insulin-like peptide-2* from the brain. *Aging Cell* **11**, 978–985 (2012).
53. Wang, Y., Azevedo, S. V., Hartfelder, K. & Amdam, G. V. Insulin-like peptides (AmILP1 and AmILP2) differentially affect female caste development in the honey bee (*Apis mellifera* L.). *Journal of Experimental Biology* **216**, 4347–4357 (2013).
54. Poitout, V. *et al.* Regulation of the insulin gene by glucose and fatty acids. *The Journal of Nutrition* **136**, 873–876 (2006).
55. Miluzio, A. *et al.* Translational control by mTOR-independent routes: how eIF6 organizes metabolism. *Biochem Soc Trans* **44**, 1667–1673 (2016).
56. Wang, X. & Proud, C. G. Nutrient control of TORC1, a cell-cycle regulator. *Trends in Cell Biology* **19**, 260–267 (2009).
57. Martin, N. *et al.* Honey bee caste lipidomics in relation to life-history stage and the long life of the queen. *Journal of Experimental Biology* **222**, (2019).
58. Munro, D. & Blier, P. U. The extreme longevity of *Arctica islandica* is associated with increased peroxidation resistance in mitochondrial membranes. *Aging Cell* **11**, 845–855 (2012).
59. Kuhnlein, R. P. Lipid droplet-based storage fat metabolism in *Drosophila*. *J. Lipid Res.* jlr. R024299 (2012).
60. Gilbert, L. I. & Chino, H. Transport of lipids in insects. *J. Lipid Res.* **15**, 439–456 (1974).
61. Gems, D. & Partridge, L. Genetics of longevity in model organisms: debates and paradigm shifts. *Annu. Rev. Physiol.* **75**, 621–644 (2013).
62. De Fine Licht, H. H., Andersen, A. & Aanen, D. K. *Termitomyces* sp. associated with the termite *Macrotermes natalensis* has a heterothallic mating system and multinucleate cells. *Mycological Research* **109**, 314–318 (2005).
63. Uys, V. M. & Plant Protection Research Institute (South Africa). *A guide to the termite genera of Southern Africa* No. 15. (Plant Protection Research Institute, Agricultural Research Council, 2002).
64. Mitchell, J. D. Colony Foundation and the development of incipient laboratory colonies of *Macrotermes natalensis* (Haviland) (Termitidae: Macrotermitinae). *afen* **28**, 215–224 (2020).

65. Sillam-Dussès, D. *Trail pheromones and sex pheromones in termites*. (Nova Science Publishers/Novinka, 2010).
66. Licht, H. H. D. F., Boomsma, J. J. & Aanen, D. K. Presumptive horizontal symbiont transmission in the fungus-growing termite *Macrotermes natalensis*. *Molecular Ecology* **15**, 3131–3138 (2006).
67. Roisin, Y. Diversity and Evolution of Caste Patterns. In *Termites: Evolution, Sociality, Symbioses, Ecology* (eds. Abe, T., Bignell, D. E. & Higashi, M.) 95–119 (Springer Netherlands, 2000).
68. Noirot, Ch. The Caste System in Higher Termites. In *Caste Differentiation in Social Insects* Ch. 6 (eds. Watson, J. A. L., Okot-kotber, B. M. & Noirot, CH.) 75–86 (Pergamon, 1985).
69. Keller, L. Queen lifespan and colony characteristics in ants and termites. *Insectes soc.* **45**, 235–246 (1998).
70. Folmer, O., Black, M., Hoeh, W., Lutz, R. & Vrijenhoek, R. DNA primers for amplification of mitochondrial cytochrome c oxidase subunit 1 from diverse metazoan invertebrates. *Molecular Marine Biology and Biotechnology* (1994).
71. Kim, D., Paggi, J. M., Park, C., Bennett, C. & Salzberg, S. L. Graph-based genome alignment and genotyping with HISAT2 and HISAT-genotype. *Nature Biotechnology* **37**, 907–915 (2019).
72. Anders, S., Pyl, P. T. & Huber, W. HTSeq—a Python framework to work with high-throughput sequencing data. *Bioinformatics* **31**, 166–169 (2015).
73. Love, M. I., Huber, W. & Anders, S. Moderated estimation of fold change and dispersion for RNA-seq data with DESeq2. *Genome Biol* **15**, 550 (2014).
74. Shannon, P. *et al.* Cytoscape: A Software environment for integrated models of biomolecular interaction networks. *Genome Res.* **13**, 2498–2504 (2003).
75. Alexa, A. & Rahnenfuhrer, J. topGO: Enrichment analysis for Gene Ontology. R package version 2.28. 0. *BioConductor. Published online* (2016).
76. Harrison, M. C. *et al.* Hemimetabolous genomes reveal molecular basis of termite eusociality. *Nature Ecology & Evolution* **2**, 557–566 (2018).
77. Li, L., Stoeckert, C. J. & Roos, D. S. OrthoMCL: Identification of ortholog groups for eukaryotic genomes. *Genome Res.* **13**, 2178–2189 (2003).
78. Slater, G. S. C. & Birney, E. Automated generation of heuristics for biological sequence comparison. *BMC Bioinformatics* **6**, 31 (2005).
79. Katoh, K. & Standley, D. M. MAFFT Multiple sequence alignment software version 7: improvements in performance and usability. *Molecular Biology and Evolution* **30**, 772–780 (2013).
80. Price, M. N., Dehal, P. S. & Arkin, A. P. FastTree: Computing large minimum evolution trees with profiles instead of a distance matrix. *Molecular Biology and Evolution* **26**, 1641–1650 (2009).
81. Letunic, I. & Bork, P. Interactive Tree Of Life (iTOL) v4: recent updates and new developments. *Nucleic Acids Res* **47**, W256–W259 (2019).
82. Khodayari, S., Moharramipour, S., Larvor, V., Hidalgo, K. & Renault, D. Deciphering the metabolic changes associated with diapause syndrome and cold acclimation in the two-spotted spider mite *tetranychus urticae*. *PLOS ONE* **8**, e54025 (2013).
83. Genitoni, J. *et al.* Hypomethylation of the aquatic invasive plant, *Ludwigia grandiflora* subsp. *hexapetala* mimics the adaptive transition into the terrestrial morphotype. *Physiologia Plantarum* **170**, 280–298 (2020).
84. McArdle, B. H. & Anderson, M. J. Fitting multivariate models to community data: a comment on distance-based redundancy analysis. *Ecology* **82**, 290–297 (2001).
85. Cajka, T., Smilowitz, J. T. & Fiehn, O. Validating quantitative untargeted lipidomics

974 across nine liquid chromatography–high-resolution mass spectrometry platforms. *Anal.*
975 *Chem.* **89**, 12360–12368 (2017).
976 86. Merlier, F., Imatoukene, N., Octave, S., Nicaud, J.-M. & Thomasset, B. A gas
977 chromatography full scan high resolution Orbitrap mass spectrometry method for
978 separation and characterization of 3-hydroxymethyl pyridine ester of fatty acids at low
979 levels. *Journal of Chromatography A* **1575**, 72–79 (2018).
980 87. Ulmer, C. Z., Patterson, R. E., Koelmel, J. P., Garrett, T. J. & Yost, R. A. A Robust
981 Lipidomics workflow for mammalian cells, plasma, and tissue using liquid-
982 chromatography high-resolution tandem mass spectrometry. in *Lipidomics: Methods*
983 *and Protocols* (ed. Bhattacharya, S. K.) 91–106 (Springer, 2017).
984 88. Tsugawa, H. *et al.* A lipidome atlas in MS-DIAL 4. *Nature Biotechnology* **38**, 1159–
985 1163 (2020).
986 89. Van den Boogaart, K. G., & Tolosana-Delgado, R. *Analyzing compositional data with*
987 *R* Vol. 122 (Heidelberg: Springer 2013).
988

FIGURE LEGENDS

Figure 1: Overview of the model system. (a) Timeline of the different stages of *Macrotermes natalensis* colonies founded from one male and one female imago each (T0). Queens from incipient laboratory colonies were sampled at 3 months after colony establishment (T1), 9 months (T2) and 31 months (T3). Field termite colonies over 20 years old are added. From field colonies, queens, workers and kings were sampled. Wild oats were supplied to the laboratory colonies from 3 months onward and the fungus *Termitomyces sp.* was introduced artificially in 3.5 months old colonies. Wood was supplied from 4.5 months onward. The drawings represent winged imagoes, workers, kings and queens at the different stages (physogastric queens become larger). Replication and sampling in our incipient colonies is further described in Supplementary Table 9. **(b)** Principal component analyses (PCAs) of gene expression across 25 samples, spanning 6 colonies, 3 castes and 5 queen stages (FW, QT0, QT1, QT2, QT3, QT4, KT4). Scores for the two main PCs are shown for all data (left) and among reproductives (i.e., without FW; right). **(c)** Weighted Gene Co-expression Network analysis (WGCN). Nine modules were detected, each represented by a color (rows). In the left-hand heatmap correlation coefficients and *p*-values are shown, relating gene expression (first major axis of the expression matrix) of each module to each caste and queen stage (columns). Positive correlations are red and negative correlations are blue; significant correlation values ($p < 0.05$) have a green border. Module size is also shown, reflecting the number of genes assigned to each module. Module expression profiles show mean expression of each module within each caste and queen stage. Enriched GO-terms of each module are displayed as tag-clouds, in which font size is inversely related to *p*-value. A visualization of the network is displayed on the right with nodes colored by their module membership. This network was created with Cytoscape (version 3.8.0) on a reduced representation of the WGCN containing the top connected genes.

Figure 2: Caste related changes in gene expression. Heatmap representing standardized gene expression (blue = low; red = high) in fat bodies of FW, QT4 and KT4. Annotations to the right of the heatmap include WGCN module (Fig. 1), gene names and gene acronyms in *Drosophila melanogaster* (right) and *Homo sapiens* (left). The map is restricted to expression of genes involved in metabolic signaling, lipid metabolism, mitochondrial oxidative phosphorylation system (OXPHOS), mitochondrial ribosome (mt-ribo), mitochondrial fission (mt-fission), mitochondrial transport (mt-transport), antioxidant defense (AO-def) and DNA repair. Expression of all genes differ significantly between FW versus QT4 and between FW versus KT4. The number of replicates per group is provided in Supplementary Table 9.

Figure 3: Cytoscape during adult queen maturation. Changes of gene expression within the gene co-expression network (GCN) with queen differentiation. Node color represents the standardized gene expression within each queen stage (low=blue: high=red). Genes that are significantly up- or down-regulated at each queen stage have a strong, black border. Enriched GO-terms within each group of up- or down-regulated genes are displayed as tag clouds below each network.

Figure 4: Heatmap with the expression of genes in fat bodies during adult queen maturation involved in lipid metabolism. Heatmap representing standardized gene expression (blue = low; red = high) at each of the five queen stages (QT0-QT4). Annotations to the right of the heatmap include WGCN module (Fig. 1), gene name and gene acronyms in *Drosophila melanogaster* (right) and *Homo sapiens* (left). Number of replicates per group is provided in Supplementary Table 9. Greater than or less than symbols (>/<) represent significant differences in expression.

Figure 5: Changes in DNA content of fat body cells during adult queen sexual maturation. Percentages of nuclear 2C, 4C and 8C cells in the fat bodies of queens in different stages (QT0 to QT4). The ternary graph shows the actual data points with stages distinguished by a colour code. The table lists per stage the average percentages of 2C, 4C, 8C. Number of replicates per group are provided in Supplementary Table 9. The proportions of cells with different DNA content differ between stages (compositional perMANOVA, $p = 0.001$), and in particular stages QT0 and QT2 differ from QT4 (post-hoc perMANOVA, both $p = 0.02$).

Figure 6: Canonical discriminant analysis of concentrations of metabolites. Three canonical functions discriminate ages and castes significantly, of which we show scores for the first two. Average scores for each caste and age are shown, plus canonical structure coefficients of each metabolite as vectors from the origin. These are proportional in length to the magnitudes of the correlations of each metabolite with the scores of the discriminant functions and show how information from each metabolite aids in discriminating castes and ages. Numbers of replicates per group are provided in Supplementary Table 9.

Figure 7: Comparison of lipid profiles between FW and QT4 in hemolymph. (a) Hierarchical clustering heatmap analysis of triglycerides (TG, orange), diglycerides (DG, green), phosphatidylethanolamine (PE, black), phosphatidylcholine (PC, grey), lysophosphatidylcholine (LPC, yellow), sphingomyelin (SM, blue) lipids in hemolymph of FW and QT4 performed in MetaboAnalyst 4.0. Individual lipids are shown in rows and samples displayed in columns, according to cluster analysis (Euclidian distance was used and Ward's clustering algorithm). Each colored cell on the heatmap plot corresponds to a normalized lipid amount above (red) or below (blue) the mean concentration for a given lipid. **(b)** Fatty acid percentages in hemolymph of FW and QT4. Percentage (%) of saturated fatty acids (SFA),

1063 monounsaturated fatty acids (MUFA) and polyunsaturated fatty acids (PUFA) of total FA in
1064 hemolymph. Ternary graph showing the percentage of SFA (orange), MUFA (black) and PUFA
1065 (blue). A permutational MANOVA found that SFA/MUFA/PUFA proportions in hemolymph
1066 were not significant different between FW and QT4. Numbers of replicates per group are
1067 provided in Supplementary Table 9.

1068

1069 **Figure 8: Changes in lipid profiles in fat bodies during adult queen maturation. (a)**
1070 Hierarchical clustering heatmap analysis of triglycerides (TG, orange), diglycerides (DG,
1071 green), phosphatidylethanolamine (PE, black), phosphatidylcholine (PC, grey),
1072 lysophosphatidylcholine (LPC, yellow), sphingomyelin (SM, blue) lipids in fat body of
1073 different stage of queen (QT0, QT2 and QT4) performed in MetaboAnalyst 4.0. Individual
1074 lipids are shown per row and mean of lipid amount of each stage displayed in columns,
1075 according to cluster analysis (Euclidean distance and Ward's algorithm). Each colored cell on
1076 the heatmap plot corresponds to a normalized lipid amount above (red) or below (blue) the
1077 mean concentrations for a given lipid. **(b)** Fatty acid percentages of different queen maturation
1078 stages (QT0, QT2, QT4) in fat body. Percentage (%) of saturated fatty acids (SFA),
1079 monounsaturated fatty acids (MUFA) and polyunsaturated fatty acids (PUFA) of total FA in
1080 fat body. Ternary graph showing the percentage of SFA (orange), MUFA (black) and PUFA
1081 (blue). The table below shows the averages of MUFA, SFA and PUFA for each stage.
1082 Permutational MANOVA demonstrated that SFA/MUFA/PUFA proportions in fat bodies of
1083 QT2 and QT4 were significantly different relative to QT0 (Permutational MANOVA, p-value
1084 = 0.012). **(c)** Box plot illustrating the peroxidation index of fat bodies of different queen
1085 maturation stages (QT0, QT2 and QT4). A box consists of upper and lower hinges and a center
1086 line corresponding to the 25th percentile, the 75th percentile and the median, respectively.
1087 Rhombuses represent the averages. Different letters indicate significantly different values

1088 according to a Kruskal-Wallis test followed by Dunn tests. Statistical differences are given for

1089 $p < 0.05$. Number of replicates per group are provided in Supplementary Table 9.

a

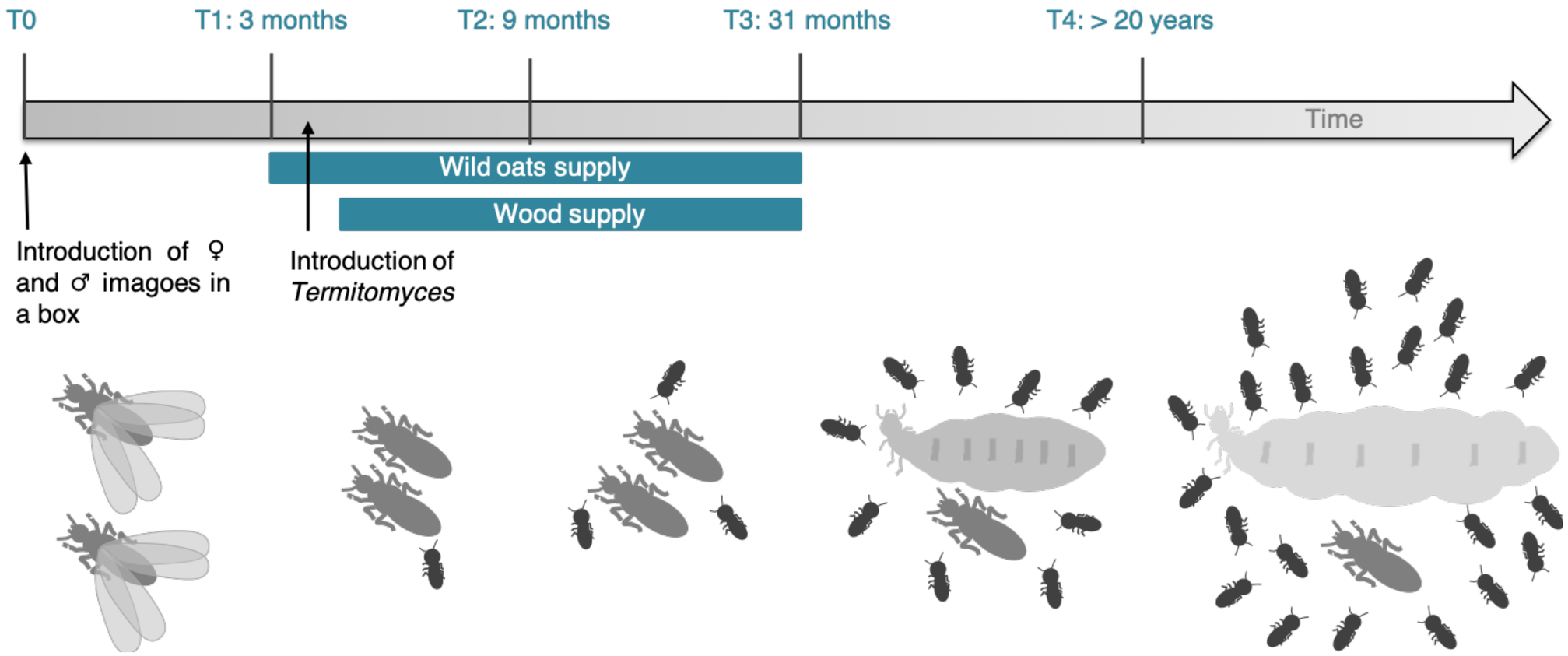

b

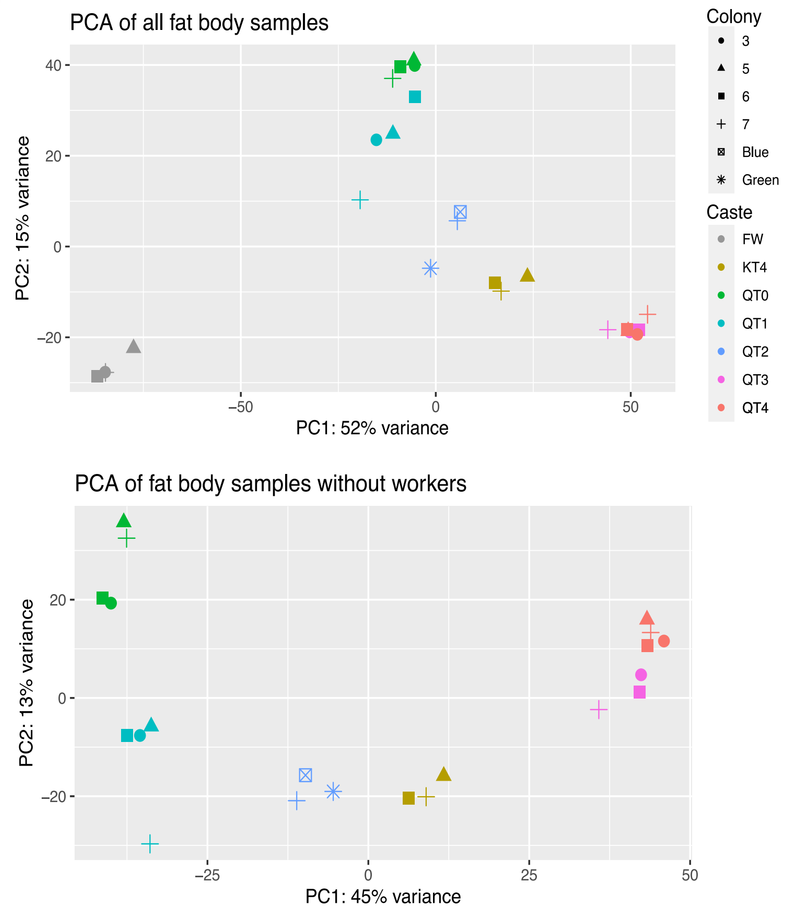

c

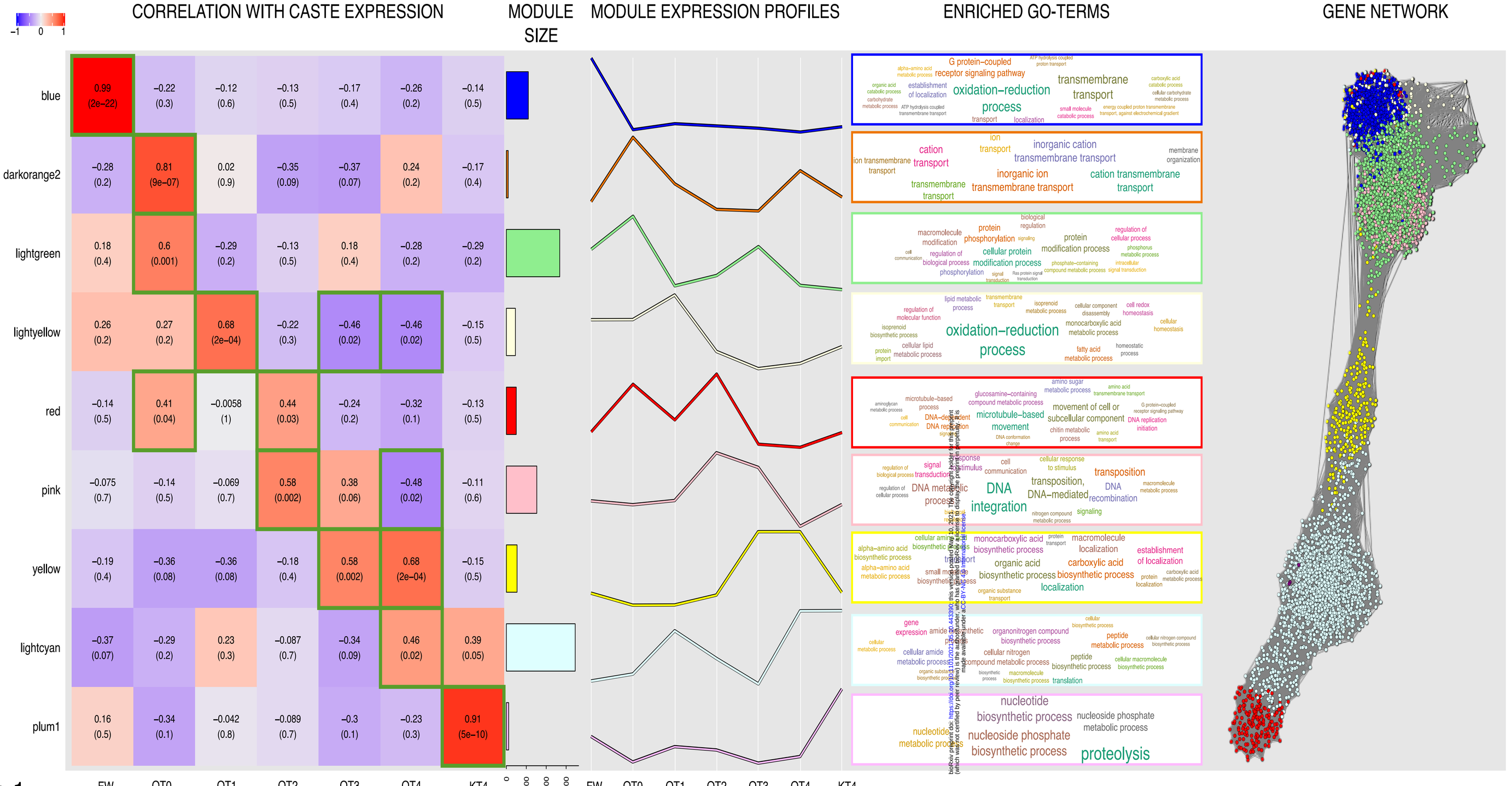

Figure 1

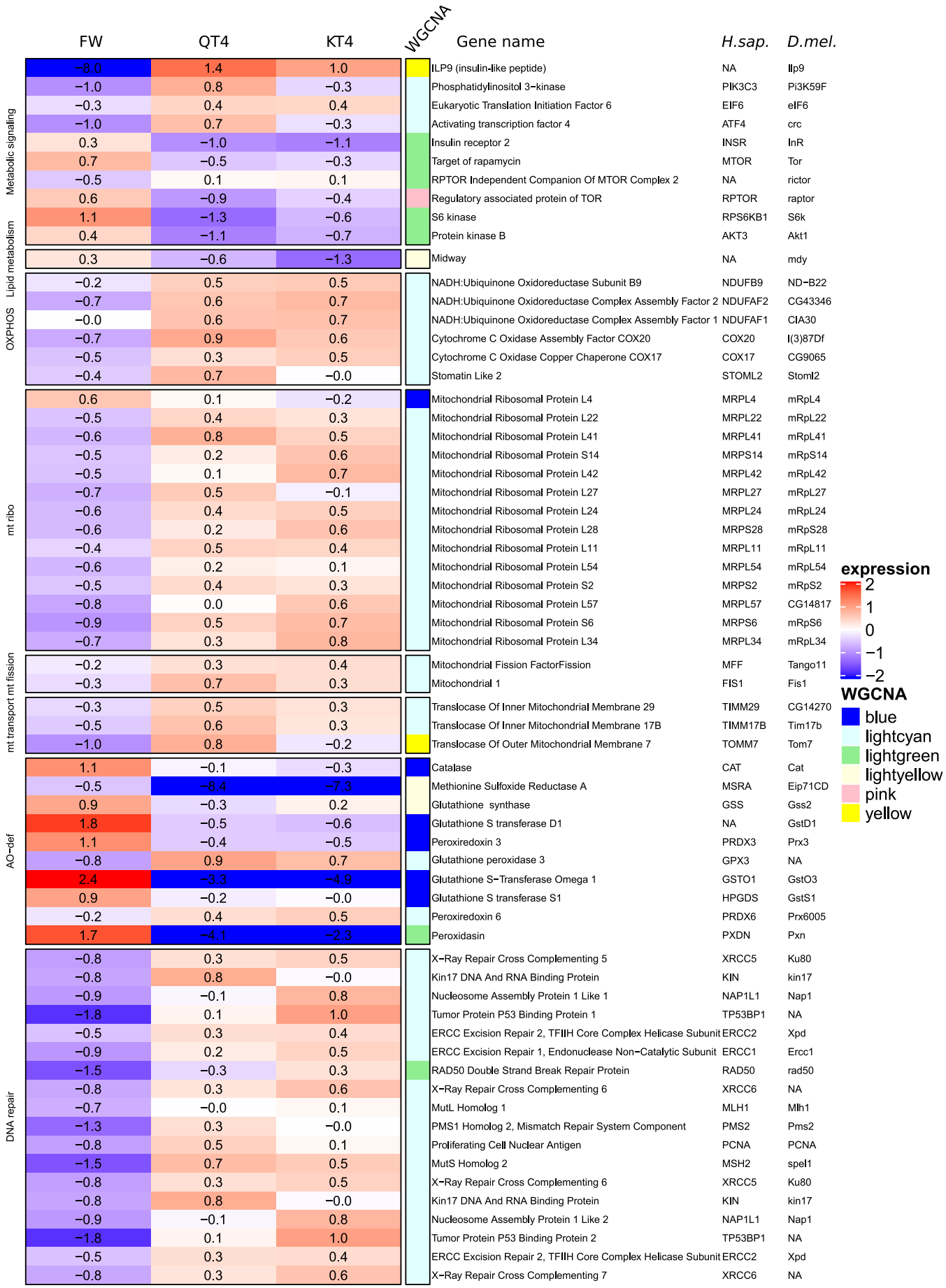
FW
QT4
KT4
WGCNA
Gene name
H.sap.
D.mel.
Metabolic signaling
Lipid metabolism
OXPHOS
mt ribo
mt transport mt fission
AO-def
DNA repair
ILP9 (insulin-like peptide) NA Ilp9
Phosphatidylinositol 3-kinase PIK3C3 Pi3K59F
Eukaryotic Translation Initiation Factor 6 EIF6 eIF6
Activating transcription factor 4 ATF4 crc
Insulin receptor 2 INSR InR
Target of rapamycin MTOR Tor
RPTOR Independent Companion Of MTOR Complex 2 NA rictor
Regulatory associated protein of TOR RPTOR raptor
S6 kinase RPS6KB1 S6k
Protein kinase B AKT3 Akt1
Midway NA mdy
NADH:Ubiquinone Oxidoreductase Subunit B9 NDUFB9 ND-B22
NADH:Ubiquinone Oxidoreductase Complex Assembly Factor 2 NDUFAF2 CG43346
NADH:Ubiquinone Oxidoreductase Complex Assembly Factor 1 NDUFAF1 CIA30
Cytochrome C Oxidase Assembly Factor COX20 COX20 l(3)87Df
Cytochrome C Oxidase Copper Chaperone COX17 COX17 CG9065
Stomatin Like 2 STOML2 Stoml2
Mitochondrial Ribosomal Protein L4 MRPL4 mRpL4
Mitochondrial Ribosomal Protein L22 MRPL22 mRpL22
Mitochondrial Ribosomal Protein L41 MRPL41 mRpL41
Mitochondrial Ribosomal Protein S14 MRPS14 mRpS14
Mitochondrial Ribosomal Protein L42 MRPL42 mRpL42
Mitochondrial Ribosomal Protein L27 MRPL27 mRpL27
Mitochondrial Ribosomal Protein L24 MRPL24 mRpL24
Mitochondrial Ribosomal Protein L28 MRPS28 mRpS28
Mitochondrial Ribosomal Protein L11 MRPL11 mRpL11
Mitochondrial Ribosomal Protein L54 MRPL54 mRpL54
Mitochondrial Ribosomal Protein S2 MRPS2 mRpS2
Mitochondrial Ribosomal Protein L57 MRPL57 CG14817
Mitochondrial Ribosomal Protein S6 MRPS6 mRpS6
Mitochondrial Ribosomal Protein L34 MRPL34 mRpL34
Mitochondrial Fission FactorFission MFF Tango11
Mitochondrial 1 FIS1 Fis1
Translocase Of Inner Mitochondrial Membrane 29 TIMM29 CG14270
Translocase Of Inner Mitochondrial Membrane 17B TIMM17B Tim17b
Translocase Of Outer Mitochondrial Membrane 7 TOMM7 Tom7
Catalase CAT Cat
Methionine Sulfoxide Reductase A MSRA Eip71CD
Glutathione synthase GSS Gss2
Glutathione S transferase D1 NA GstD1
Peroxiredoxin 3 PRDX3 Prx3
Glutathione peroxidase 3 GPX3 NA
Glutathione S-Transferase Omega 1 GSTO1 GstO3
Glutathione S transferase S1 HPGDS GstS1
Peroxiredoxin 6 PRDX6 Prx6005
Peroxidasin PXDN Pxn
X-Ray Repair Cross Complementing 5 XRCC5 Ku80
Kin17 DNA And RNA Binding Protein KIN kin17
Nucleosome Assembly Protein 1 Like 1 NAP1L1 Nap1
Tumor Protein P53 Binding Protein 1 TP53BP1 NA
ERCC Excision Repair 2, TFIIH Core Complex Helicase Subunit ERCC2 Xpd
ERCC Excision Repair 1, Endonuclease Non-Catalytic Subunit ERCC1 Ercc1
RAD50 Double Strand Break Repair Protein RAD50 rad50
X-Ray Repair Cross Complementing 6 XRCC6 NA
MutL Homolog 1 MLH1 Mlh1
PMS1 Homolog 2, Mismatch Repair System Component PMS2 Pms2
Proliferating Cell Nuclear Antigen PCNA PCNA
MutS Homolog 2 MSH2 spel1
X-Ray Repair Cross Complementing 6 XRCC5 Ku80
Kin17 DNA And RNA Binding Protein KIN kin17
Nucleosome Assembly Protein 1 Like 2 NAP1L1 Nap1
Tumor Protein P53 Binding Protein 2 TP53BP1 NA
ERCC Excision Repair 2, TFIIH Core Complex Helicase Subunit ERCC2 Xpd
X-Ray Repair Cross Complementing 7 XRCC6 NA
expression
2
1
0
−1
−2
WGCNA
blue
lightcyan
lightgreen
lightyellow
pink
yellow

Figure 2

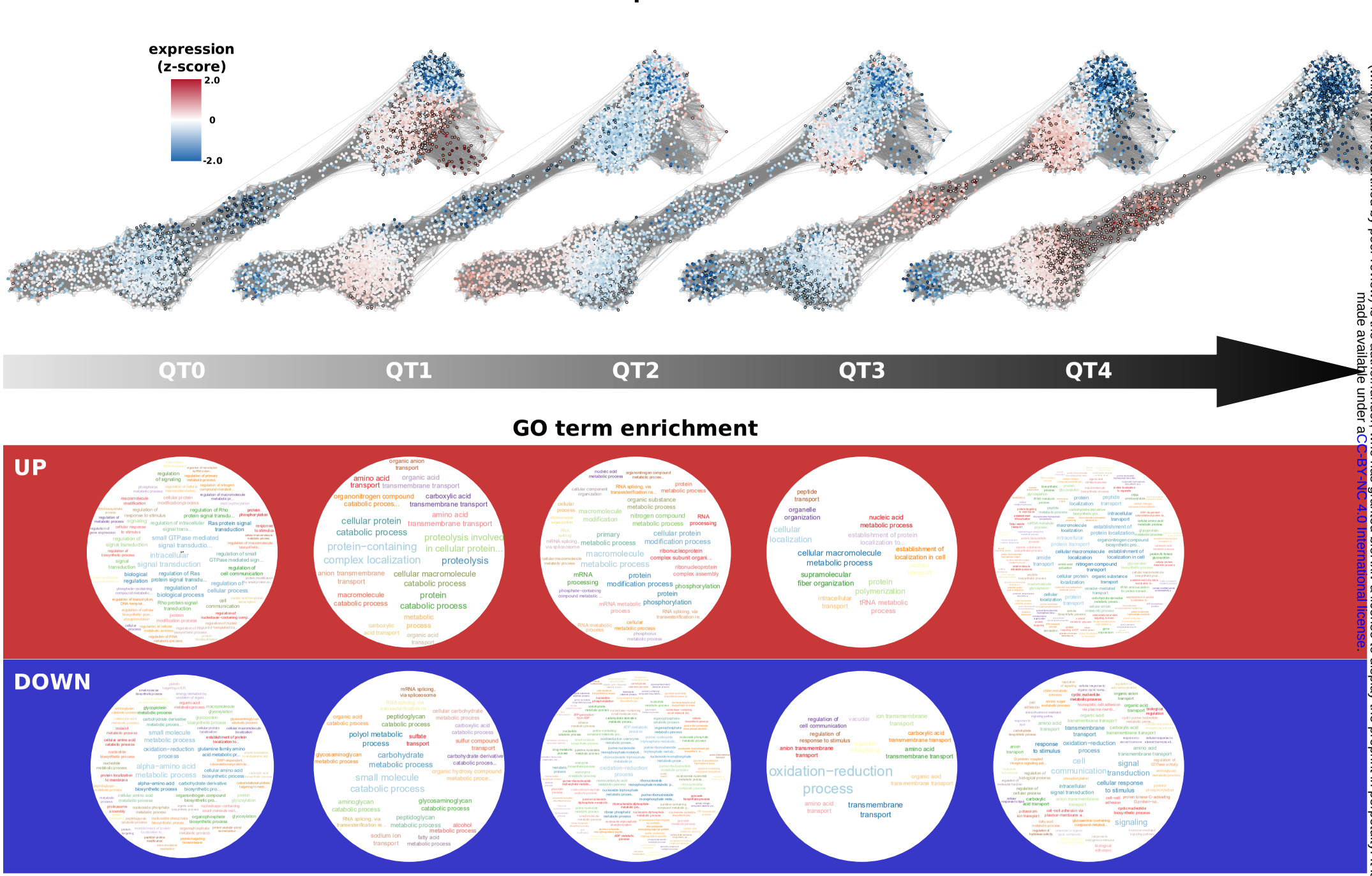

Figure 3

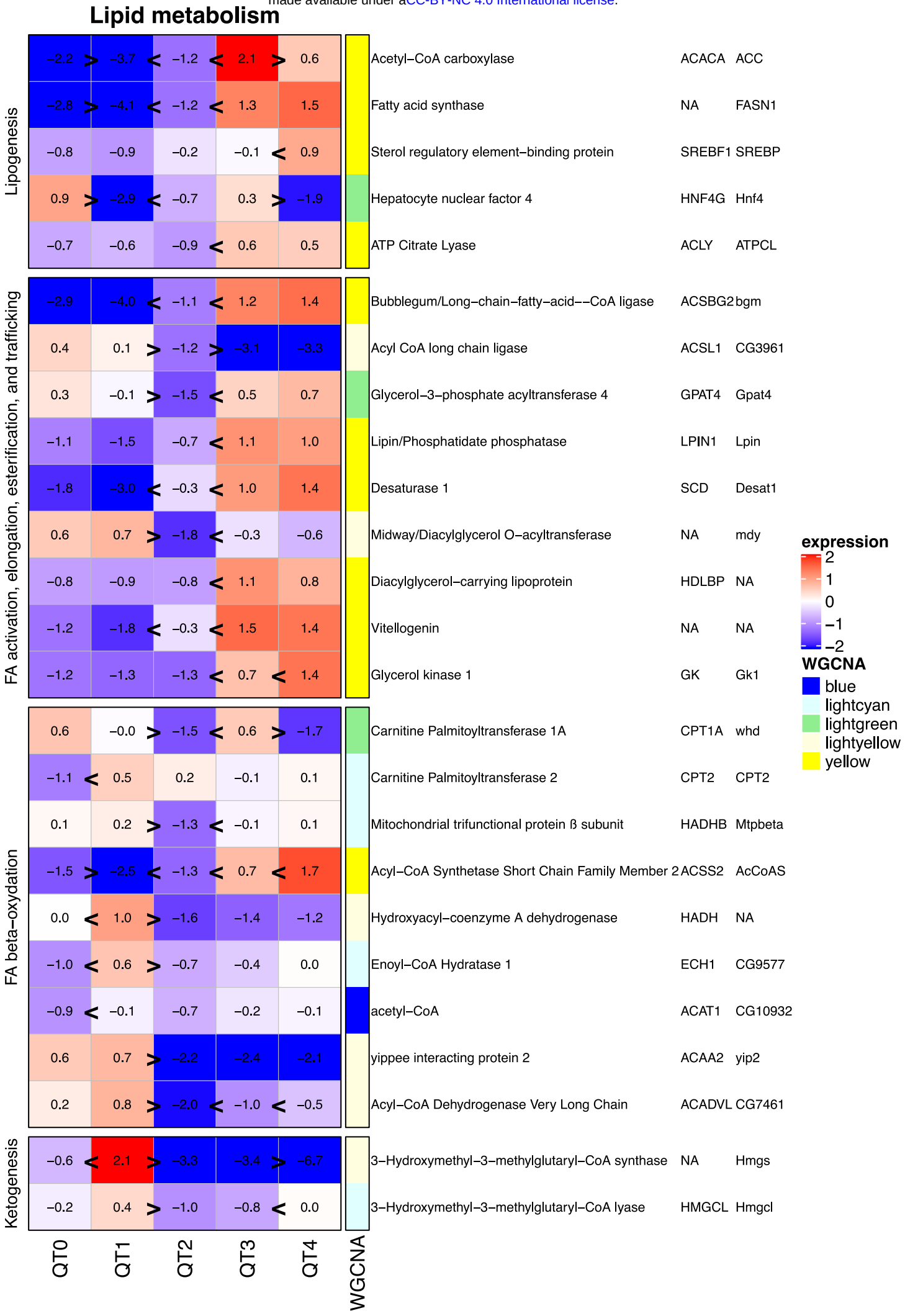

Figure 4

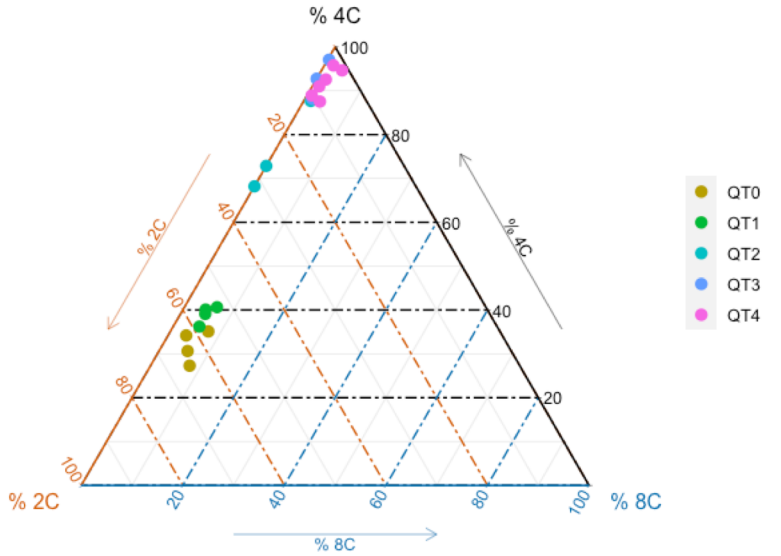

	QT0	QT1	QT2	QT3	QT4
2C (%)	62.1	55.8	23.3	6.8	5.9
4C (%)	31.8	39.0	76.2	92.7	91.4
8C (%)	6.1	5.2	0.5	0.6	2.6

Figure 5

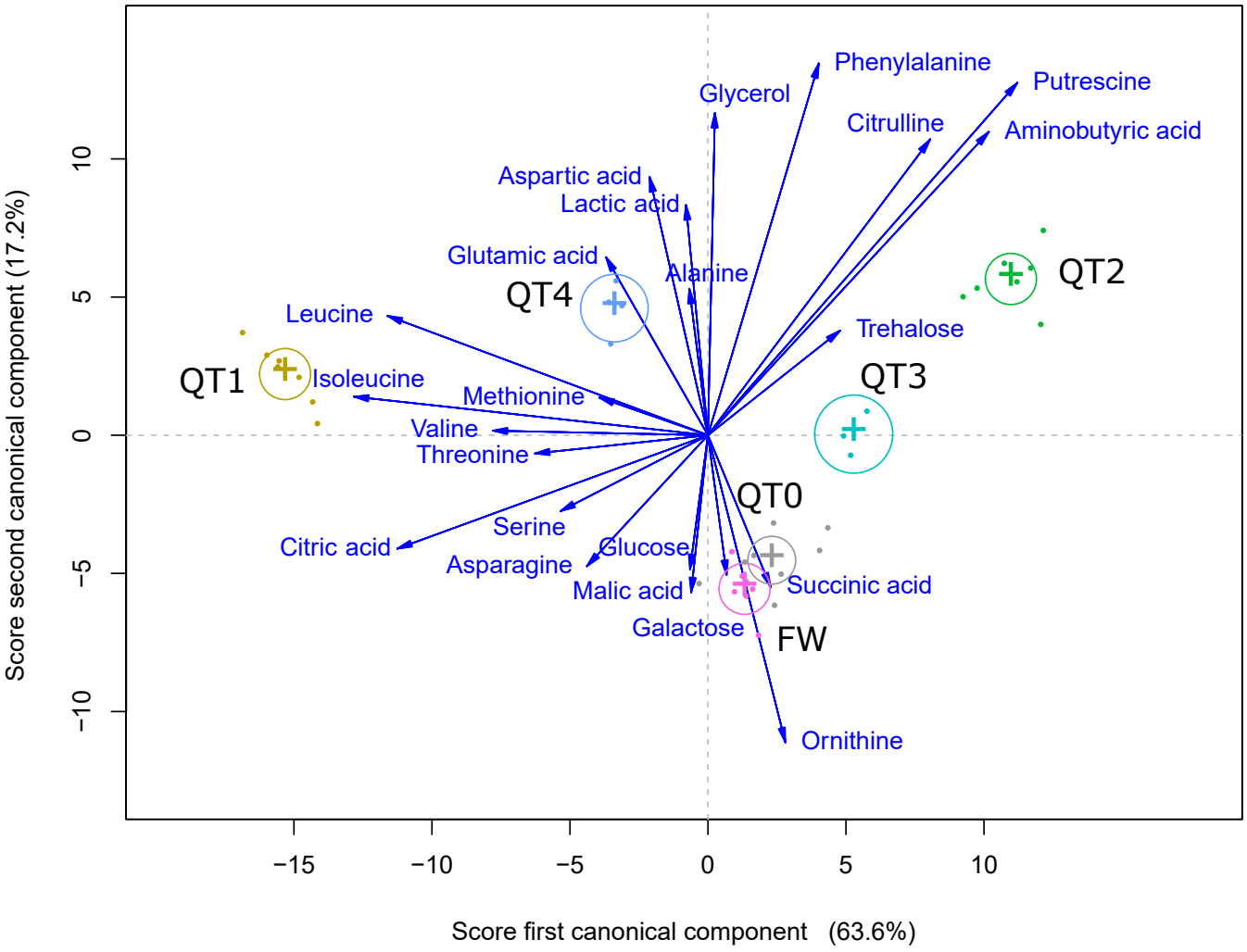
Phenylalanine
Putrescine
Glycerol
Citrulline
Aminobutyric acid
Aspartic acid
Lactic acid
Glutamic acid
Alanine
QT2
QT4
Leucine
Trehalose
QT1
Isoleucine
QT3
Methionine
Valine
Threonine
QT0
Serine
Citric acid
Glucose
Asparagine
Succinic acid
Malic acid
Galactose
FW
Ornithine
Score second canonical component (17.2%)
Score first canonical component (63.6%)
10
5
0
−5
−10
−15
−10
−5
0
5
10

Figure 6

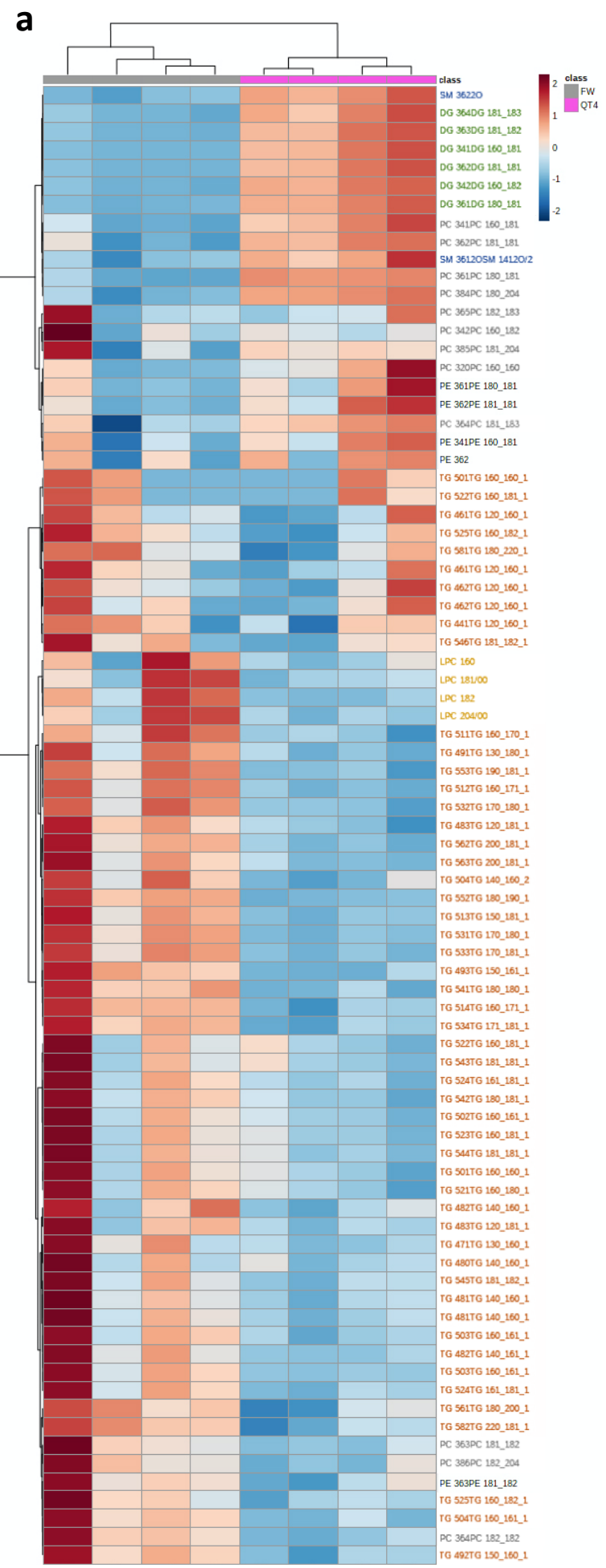

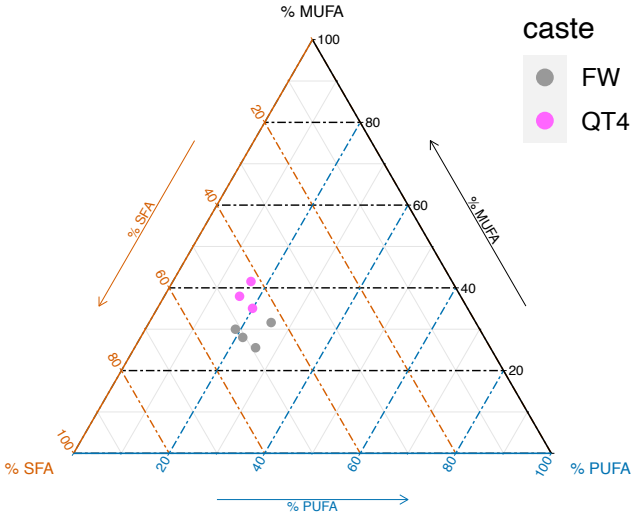

	FW	QT4
SFA (%)	48.43	44.47
MUFA (%)	28.79	38.18
PUFA (%)	22.78	17.34

Figure 7

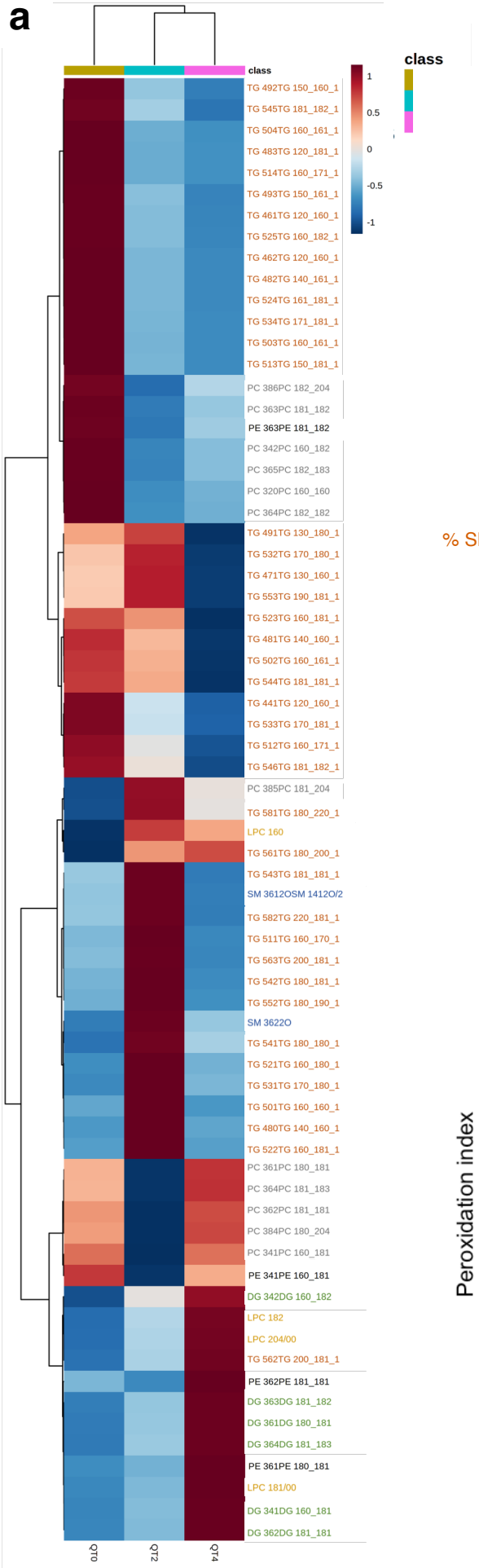

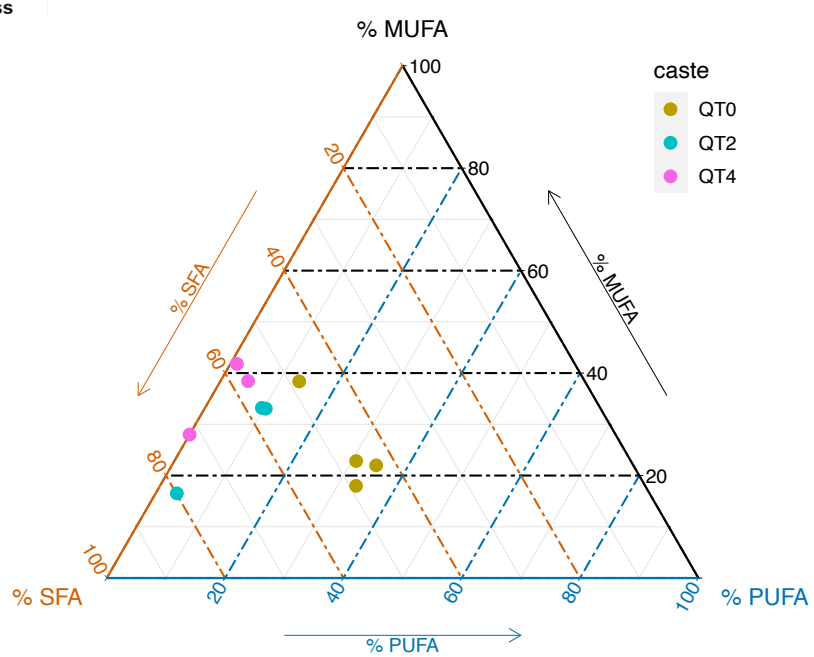

	QT0	QT2	QT4
SFA (%)	46.77	64.55	62.00
MUFA (%)	25.30	27.60	36.08
PUFA (%)	27.94	7.85	1.92

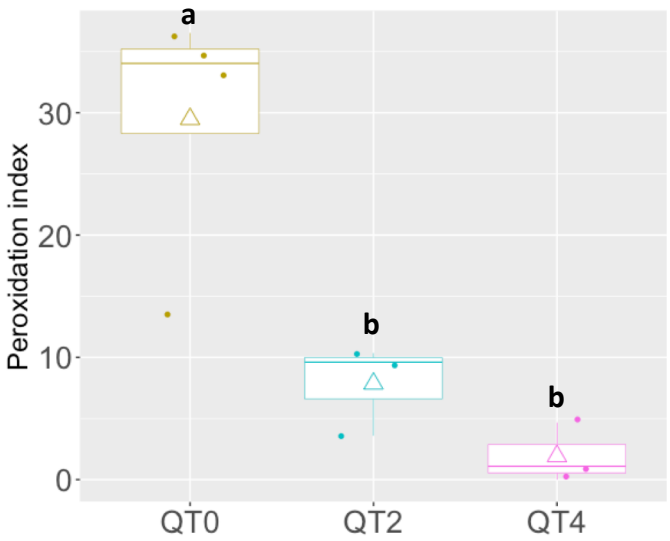

Figure 8